Mémoire

Auteur : Bau, Sébastien
Promoteur(s) : 8567; Grodent, Denis
Faculté : Faculté des Sciences
Diplôme : Master en sciences spatiales, à finalité spécialisée
Année académique : 2022-2023
URI/URL : http://hdl.handle.net/2268.2/18704

Royal Observatory of Belgium

Hypervelocity Impact Modelling

Impact Craters and Gravitation on the Didymos Asteroid's Moonlet Dimorphos

16 August 2023

Sébastien A.V. BAU

The University of Liège
Faculty of Sciences
Master in Space Sciences
Professional focus

Academic year 2022-2023

University supervisor(s) :
Dr Denis GRODENT
d.grodent@uliege.be

Promotor(s) :
Dr Cem Berk SENEL
cem.berk@observatory.be
Dr Özgür KARATEKIN
ozgur.karatekin@observatory.be

Reading committee:
Grodent, Denis; Karatekin, Özgür; Rauw, Gregor; Senel, Cem Berk

Reader(s):
Dr Véronique DEHANT
v.dehant@oma.be

LIÈGE université Sciences

This thesis work contains many figures and pictures. Please think of the environment before printing.

Contents

1 Introduction **5**
1.1 The Asteroids . . . 5
Didymos . . . 5
Orbit . . . 5
Rotation . . . 6
Dimorphos . . . 8
Mass . . . 9
1.2 DART Mission . . . 9
Impact . . . 11
1.3 Hera Mission . . . 11
Gravimetry . . . 12
1.4 Thesis Goals . . . 13
Scientific Goals . . . 13
Didactic Goals . . . 13

2 Theoretical Background **14**
2.1 Physical Parameters . . . 14
Cohesion . . . 14
Porosity . . . 14
2.2 Gravity Anomaly . . . 16
Free-air anomaly . . . 18
Bouguer anomaly . . . 18
Other anomalies . . . 18
Units . . . 18

3 Methodology **19**
3.1 DART Parameters . . . 20
3.2 iSALE-Dellen . . . 21
2D Simulation . . . 23
3.3 pySALEPlot . . . 25
Post-processing . . . 25
3.4 Polyhedron Gravity Model . . . 26

4 Results & Discussion **28**
4.1 2D Simulations . . . 28
Gravity Anomalies . . . 32
4.2 Gravity Shape Models . . . 38

5 Conclusion **42**
5.1 Improvements & Future Work 42
Afterword 43

Acknowledgements **44**

Abbreviations **44**

References **45**

A Appendix **50**
A.1 Thesis Topic Proposal 50
A.2 Initial iSALE2D Plots 50
A.3 More iSALE Plots 53
A.4 Gravity Shape Model Images 56
A.5 Example iSALE Input Files 58
50% 100 kPa 58
30% 10 kPa 60
10% 1 kPa 62
10% 100 kPa 63
10% 10 kPa 65

List of Figures

1 Taken from Fig. 9.20 of *Planetary Sciences* p393, showing the spin rate limit for gravitationally-bound bodies with densities of 3 g · cm^{-3} [9] 7
2 Crater geometries: $h/a = 1$ concentric crater,$h/a = 8$ flat-bottomed, $h/a = 12$ central-mound, $h/a = 20$ bowl-shaped/normal. h is the regolith thickness and a is the impactor radius. Taken from Figure 5 in Raducan et al. 2020 [25] 15
3 Lunar (top) and laboratory (bottom) crater geometries. Taken from Fig. 1 in Quaide & Oberbeck 1968 [24] 16
4 From Figure 1 of "Gravity, Data to Anomalies" *Encylopedia of Solid Earth Geophysics*, p524-533 [13] 17
5 From figure 2 of "Gravity, Data to Anomalies" *Encylopedia of Solid Earth Geophysics* , p524-533 [13] 19
6 1 kPa cases courtesy of Robert Luther and co-authors [22] 27
7 10 kPa cases courtesy of Robert Luther and co-authors [22] 27
8 100 kPa cases courtesy of Robert Luther and co-authors [22] 27
9 100 kPa crater evolution and contour plots of porosity and density . . 29

10 10 kPa crater evolution and contour plots of porosity and density . . 30
11 1 kPa crater evolution and contour plots of porosity and density . . . 31
12 Bouguer anomalies for 10% 1 kPa case 33
13 Bouguer anomalies for 30% 1 kPa case 33
14 Bouguer anomalies for 50% 1 kPa case 34
15 Bouguer anomalies for 10% 10 kPa case 34
16 Bouguer anomalies for 30% 10 kPa case 35
17 Bouguer anomalies for 50% 10 kPa case 35
18 Bouguer anomalies for 10% 100 kPa case 36
19 Bouguer anomalies for 30% 100 kPa case 37
20 Bouguer anomalies for 50% 100 kPa case 37
21 Small Body Mapping Tool (SBMT) colour map of $Y = 100$ kPa, $\phi = 30\%$ case 39
22 Small Body Mapping Tool (SBMT) colour map of $Y = 10$ kPa, $\phi = 30\%$ case 40
23 Small Body Mapping Tool (SBMT) colour map of $Y = 1$ kPa, $\phi = 30\%$ case 41
24 100 kPa cases before crater settled 51
25 10 kPa cases before crater settled 52
26 1 kPa cases before crater settled 53
27 Plots of 50% 100 kPa crater morphology evolution through time . . . 54
28 Plots of 50% 100 kPa crater morphology evolution through time . . . 55
29 SBMT map of $Y = 100$ kPa, $\phi = 50\%$, modelled from Luther et alia 2022 [22] 56
30 SBMT map of $Y = 10$ kPa, $\phi = 50\%$, modelled from Luther et alia 2022 [22] 57
31 SBMT map of $Y = 1$ kPa, $\phi = 50\%$, modelled from Luther et alia 2022 [22] 58

List of Tables

1 Taken from Table 1 of Cheng et al. 2022 [3] 10
2 *iSALE2D* impact crater simulation constant parameters and the resulting simulation plots. 20
3 Luther et al. *iSALE2D* impact crater simulations. Provided by Luther et al. 2022 from private correspondence [22]. The resulting 3D shape models can be found in Appendix A.4 20
4 Main DART parameters from literature and other simulations. 21
5 Model parameters for the iSALE2D simulations 22
6 Material parameters for the iSALE2D simulations. 23

7 Distension inputs $\alpha_0 = [1 - \phi]^{-1}$ from porosity levels for *iSALE2D* simulations [5] 24

1 Introduction

The Double Asteroid Redirection Test (DART) probe crashed into the binary companion of near-Earth asteroid Didymos in September of last year, bringing the human race closer to understanding how to protect our fragile home from possible incoming asteroid threats. The moonlet Dimorphos' size is of the order of 100 m, meaning it could destroy a city and cause a tsunami if it were to hit Earth!
But this is not what this work is going to focus on. Next to all the excitement about planetary defence, the DART and Hera missions will reveal a tremendous amount of information about asteroids and our solar system. This is the first time that we are sending gravity instruments to an asteroid. The freshly exposed DART crater will also reveal material from below the surface of this small body, revealing clues about its composition and density.
This master thesis work investigates the different craters that could have occurred on Dimorphos based on varied porosity and cohesion due to the DART impact and how these craters could influence the small body's gravitational potential, if at all.
In the following sections, I will introduce the near-Earth asteroids of concern to my work and the space missions that involve them, as they are not only relevant to the thesis topic but are the main reason why it was proposed by Dr Karatekin at the Royal Observatory of Belgium (ROB).

1.1 The Asteroids

65803 Didymos

Discovered in 1996 by a researcher called Joseph Montani in Arizona, USA, the small body 65803 Didymos is a 775 ± 80 m diameter near-Earth object (NEO). Its name, meaning "twin" in ancient Greek, was given to it in 2003 after it was discovered that it had a companion, later named Dimorphos [2]; [14]; [18]. They are estimated to both be S-type asteroids, which is a taxonomic class grouping asteroids with similar composition. The S classification groups asteroids that are "stony", with moderate albedos and spectra indicating iron and magnesium ([9] p380). They are the most common class for NEOs, including the asteroids 433 Eros and 25143 Itokawa that were visited by the *NEAR Shoemaker* and *Hayabusa 1* missions respectively. Didymos' density is estimated to be
$2.146 \pm 30\%$ g $\cdot$ cm^{-3} $= 2146$ kg $\cdot$ m^{-3} [2].

Orbital Details

The NEO has a semi-major axis a, eccentricity e and inclination i of 1.64 au, 0.384, 3.4°° respectively (Richardson et al. 2022). The orbit of Didymos about the Sun is classified as an *Amor* type orbit, or an Amor asteroid [18]. These types of NEOs have particular orbital properties similar to their archetype

asteroid: 1221 Amor. The perihelion distances of Amor types lie in the range $1.017\text{au} < q < 1.3\text{au}$ and the asteroids can have diameters as great as 30 km. They make up roughly 40% of the NEO population and are within the orbit of Mars. The *Apollo* group makes up 50% and is characterised by perihelia $q < 1.017\text{au}$. The third group is called the *Atens* and makes up less than 10% of the NEO population. These have semi-major axes $a < 1\text{au}$, aphelia greater than Earth's perihelion, i.e. $Q > 0.983\text{au}$. If a NEO's orbit is entirely within Earth's orbit around the Sun, it is classified as an *Apohele* asteroid ([9] p369).

Rotation

Didymos has an orbital period of 2.11 years about the Sun and a rotation period of 2.26 hours (about itself), which is quite fast considering its size (~ 700 m) [18]. Asteroids of the order of > 100 m have a theoretical limit of how fast they can spin without disintegrating due to the centrifugal forces: more or less 2 hours. This is because most of these bodies are incoherent objects, such as rubble piles; they are not made of a single coherent piece of rock material but are rather an aggregation of various-sized pieces due to the Solar system's dynamic past. A small and coherent body would be able to spin faster without losing much of its mass ([25]; [9] p387).
More than 80% of all planetary bodies (this is not restricted to NEOs and Main-belt asteroid (MBA)s, but also Jupiter Trojans & Greeks, Kuiper-belt object (KBO)s and dwarf planets) have rotation periods in the range of $4 - 16$ h and the size and rotation period are correlated, with bodies < 5 km spinning faster than larger ones. The fastest spinning asteroid with a size of > 1 km is 2.2 h. It is believed that the collision history of large small bodies (with radii $R \gtrapprox 60$ km) is the greatest factor contributing to their current rotation periods. Smaller bodies, especially NEOs of sizes $0.1 \lessapprox r \lessapprox 10$ km, have a seemingly excess number of slow rotators, with only 30% having a rotation period $\lessapprox 4$ h. The smallest bodies with $R \lessapprox 100$ m spin much more rapidly, such as the 15 m radius asteroid 1996 KY_{26}, which rotates about itself in about 10 minutes. Such a fast spinner suggests it is a coherent body and not a rubble pile ([9] p391-393).
Figure 1, shows the spin rate limit, i.e. the maximum rotation rate, for small bodies with a density of $3\ \text{g} \cdot \text{cm}^{-3}$ that are gravitationally bound. It includes NEOs as well as MBAs, Mars crossers and tumblers.

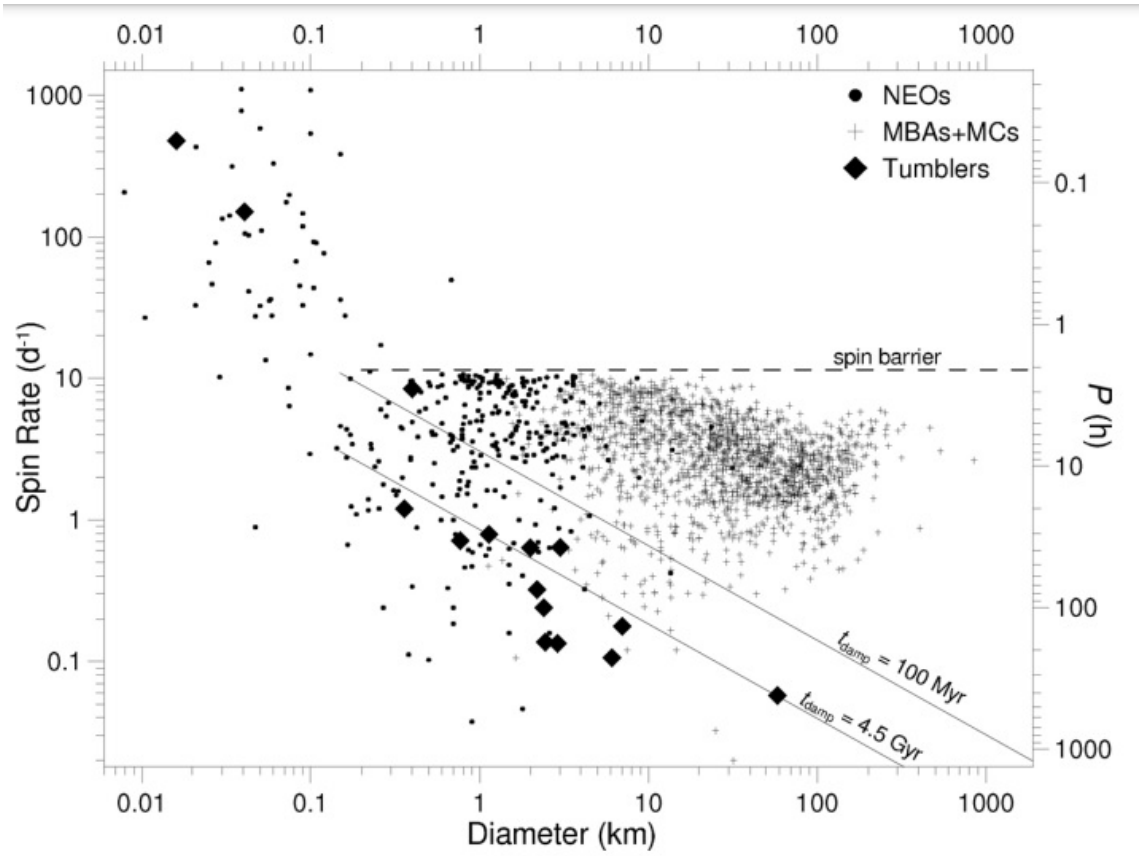

Figure 1: Taken from Fig. 9.20 of *Planetary Sciences* p393, showing the spin rate limit for gravitationally-bound bodies with densities of 3 g · cm^{-3} [9]

The atypically fast rotation rate of our Didymos translates to its shape: it has an equatorial bulge, most likely due to the material being driven towards the plane of rotation and piling up at the equator, making it look like a dreidel or spinning-top [18]. This suggests that Didymos is a rubble pile asteroid.
A rubble pile asteroid is one made up of gravitationally bound fragments and void spaces, in contrast to a coherent body. A coherent body would characteristically have high strength and low porosity, whereas a rubble pile asteroid would typically be more porous and have weaker cohesion (see Section 2.1). Evidence shows that most MBAs are rubble piles, coming from the fact that the densities of the few asteroids that have been measured were much lower than the densities of meteorites on Earth with similar spectra ([9] p387).
Rotation rates of MBAs also suggest that they are rubble piles because single coherent objects would have shorter periods than non-monolithic bodies, as the fast rotators would lose too much material from the centrifugal forces of a high spin, thus not holding together for a long time. Most asteroid families also have several large bodies of similar size, suggesting they belonged to a single-parent

body that was shattered by collisions. Simulations with this scenario of a single rubble pile reproduce the observed velocity and size distributions observed today, whereas the scenario where they all come from a parent body that is coherent and monolithic does not ([9] p387).

Dimorphos a.k.a. Didymoon

Previously called Didymos I and nicknamed "Didymoon" before it was officially renamed in 2020, Dimorphos, meaning "two forms" in ancient Greek, has a diameter of around 160 m, about the size of the Giza Pyramid. It is uncertain if it formed together with its primary Didymos, or if it is material from Didymos that was ejected during a collision, or if it comes from another body and was captured by Didymos [14]; [18].
It is not unusual for asteroids to be part of a binary system. A binary system is a pair of small bodies that are gravitationally bound such that they orbit each other. For bodies to be gravitationally bound to one another and form a binary, we need energy from the system to be removed by a third body, as having only two bodies does not lead to long-term stability. Events such as collisions and tidal interactions with a planet can produce debris that will collide or interact with the pair.
The Yarkovsky effect, which affects bodies of the order of meters to tens of kilometres, can influence the orbit of bound pairs over very long timescales. It is the effect of temperature due to solar radiation hitting a rotating body, thus warming one part of the hemisphere more than another, which leads to a force that can expand or decay the orbit of the body. The Yarkovsky–O'Keefe–Radzievskii–Paddack (YORP) effect affects bodies of sizes up to ~ 40 km and is a torque changing a body's rotation rate due to the uneven distribution of sunlight on its surface (Planetary Sciences p47-48 [9]).
The different asteroid reservoirs have different most likely scenarios that lead to the way they are today. The most likely scenario for MBAs and the Jupiter Trojans & Greeks is the collision one, whereas for NEOs it is rotational disruption. This is because NEOs have a dynamical lifetime ten times shorter than the timescale required for collisions to lead to bound pairs. NEOs could be dominated by tidal interactions with planets and YORP torques among other forms of rotational disruption ([9] p389).
The semi-major axis of Dimorphos to its primary is $a = 1.18\ (+0.04/-0.02)$ km and its orbit has the low eccentricity of $e < 0.03$ [2]. If they have a mass ratio between the two of them ≥ 3, we can call them a primary and its satellite, whereas a mass ratio < 3 would be called a binary system where the members are of equal standing gravitationally and the bodies are of comparable sizes ([9] p387).

Mass

Without knowing Dimorphos' mass, we cannot estimate this ratio. However, based on the diameter ratio of $\frac{770\ \text{m}}{160\ \text{m}} \approx 4.8$, it seems appropriate enough to call Dimorphos a satellite or a moon of its primary, as it is about 5 times smaller in size to Didymos. In fact, most papers refer to Dimorphos as the satellite or 'moonlet' of Didymos, while still referring to the system as a binary asteroid system.
There are multiple techniques to determine the mass of an asteroid, notably measuring radar echoes or using astrometric measurements. Another way is by sending a probe to the body and orbiting it. From Kepler's third law of gravitation

$$\frac{P_{orb}^2}{a^3} = \frac{4\pi^2}{G(m_1 + m_2)}$$

we can estimate the mass of the body the probe was orbiting if we know the orbital period and the semi-major axis of the 2 body problem, as well as the mass of the probe sent ([9] p23). For bound pairs, we can observe the period they orbit around each other and if we have their orbital distances about each other we get the semi-major axis of this system, which we can use to find the total mass. It follows that the estimated mass of the Didymos system is 5.28×10^{11} kg, i.e. the combined mass of both objects, Didymos and Dimorphos [28]. To constrain their respective masses we need to rely on different methods. Once the mass and the shape is known, we can determine the density of the body, revealing very useful information about the asteroid, such as its composition ([9] p389).

1.2 DART Mission

The historic DART mission is a National Aeronautics and Space Administration (NASA) probe that was launched on 24 November 2021 from California, USA, towards our pair of NEOs, Didymos and Dimorphos.
The asteroid binary system of Didymos and its moonlet Dimorphos were selected as DART's targets not because they could be a threat to Earth, but because they pass relatively close to us. We can assume it is easier to observe the system from the ground and is cheaper on fuel than to do an experiment in the Main Belt. The fact that it is a binary system would also mean that the orbital period of the satellite around the primary body can be measured more easily and accurately than trying to measure an orbital change of a single asteroid about the Sun. In 2003 (which coincides with Dimorphos' discovery), Didymos was only 0.048 au away from Earth (about 7 million km), but it can be as distant as 3 au away ($\sim$ 450 million km) when it is at the conjunction (behind the Sun from Earth's perspective, as opposed to the opposition, where the Earth would be in between it and the Sun) and slightly further than Mars' orbit [18].
The goal of the mission was to deflect an asteroid from its trajectory using the momentum transfer method, i.e. an object is shot into the asteroid, imparting

some of its momentum to it to deviate it from its usual orbit. The idea is that even a small deviation from its trajectory could potentially save it from hitting the Earth.
The main strategies for changing an asteroid's orbit include [2]:

- Kinetic impactor, i.e. impacting the body with a spacecraft and transferring momentum to it (the method followed for the DART mission)
- Gravity tractor, i.e. deviating the body from its trajectory due to the gravity of a massive spacecraft flying closeby
- Blast deflection, i.e. blasting the body with the detonation of a nuclear weapon to push it onto a new trajectory
- Surface modification or ablation, i.e. change the surface with lasers or particle beams and affect its orbit and rotation.

When planning the mission, NASA set the minimum successful orbital period change for their mission to 73 s or more. This means that if DART changed the orbit of Dimorphos by at least 73s, the mission would be deemed successful.
A 6U CubeSat, called the Light Italian Cubesat for Imaging of Asteroids (LICIACube), made by the Italian space agency, Agenzia Spaziale Italiana (ASI) was also onboard DART. It was deployed a few days before the impact to take pictures of the target as well as the ejecta cloud that would be produced during the impact on the moonlet [18]. Table 1 summarises some of the flight details of the DART mission including information about LICIACube.

LICIACube Flyby Mission Design		
LICIACube	Release from DART	10 days before DART impact
	Flyby speed relative to Didymos	6.145 km s^{-1}
	Closest approach distance to Didymos	51.2 km
	Closest approach delay from DART impact	167 s
	Time for which LEIA images are < 5 m px^{-1}	63.7 s
DART Kinetic Impact		
DART	Launch date	24 Nov 2021
	Arrival date	26 Sep 2022
	Arrival relative speed	6.145 $km\ s^{-1}$
	Maximum Earth distance	0.19 au
	Earth distance at impact	0.0757 au
	Solar distance at impact	1.046 au
	Arrival solar phase angle	59.5°
	Impact angle to binary orbit velocity	166°

Table 1: Taken from Table 1 of Cheng et al. 2022 [3]

Impact

The historic DART impact occurred on 26 September 2022 with an impact speed of ~ 6.6 km $\cdot$ s^{-1} and made Dimorphos the first body in the solar system to have its orbit shifted by a measurable amount due to human effort. The Dimorphos system was $\sim 11 \times 10^6$ km < 0.08 au from Earth at the time [14, 18].
Ground telescopes observed the change in the moonlet's orbital period about its primary. Before DART collided, Dimorphos took 11 hours and 55 minutes to orbit Didymos, or, more precisely, it had a period of 11.92 $(+0.004/-0.006)$ hours about Didymos [2]. Post-impact, the binary's orbital period about Didymos decreased by 32 minutes to 11 hours and 23 minutes. There is of course an uncertainty associated with these measurements of the order of 10% according to the European Space Agency (ESA) news page [14], while NASA wrote that the error is 32 ± 2 minutes on theirs [18]. The error will further be decreased after ESA's follow-up mission to DART comes around in 2026, called *Hera*.

1.3 Hera Mission

Hera, named after an ancient Greek goddess, is ESA's follow-up mission to NASA's DART mission. Together they are the first probes meeting up with a binary asteroid system, with DART having performed the kinetic impact and Hera planned to rendezvous with Didymos and Dimorphos for a detailed in-situ study in December of 2026 [14].
Hera's predecessor mission was called Asteroid Impact Mission (AIM) which, together with DART, made up a joint asteroid deflection mission that was dubbed Asteroid Impact & Deflection Assessment (AIDA). The joint missions were supposed to test a spacecraft's ability to impact a NEO and then measure and characterise the deflection resulting from said impact. The idea was to see exactly how well one could deflect potentially dangerous asteroids via the kinetic impact method. AIM had a planned launch of October 2020 and would go to the Didymos binary system to characterise the target in May or June of 2022, before DART, with a planned launch of December 2020, would arrive and impact it shortly after in September or October of 2022. AIM would have gathered data of the impact in-situ, with known conditions and physical properties of the target Dimorphos. N.B.: at the time of AIM, the moonlet was not yet officially named Dimorphos in the literature.
AIDA would have covered the full picture of the impact, momentum transfer, crater size and morphology and the evolution of the coma of ejecta from the impact. The return on investment would have been greatest if it was present at the binary before, during and after the DART impact.
Unfortunately, AIM was axed and eventually replaced with the Hera mission. Although it was tied to AIDA, DART was considered a stand-alone mission and did not depend on AIM to succeed. Currently, the AIDA collaboration between

ESA and NASA still stands, with Hera replacing AIM [2].
In 2018, LICIACube was added to the DART programme. It was deployed by DART a few days before impact, to make a separate flyby of the moonlet and image the coma of impact ejecta as well as to image Didymos and the hemisphere of Dimorphos opposite to the impact crater [2, 18].
As the successor of AIM, Hera will assess the crater created by the DART impact. This survey aims to learn about the effectiveness of the kinetic impactor method for asteroid deflection and make it a repeatable technique that could one day save our planet from catastrophic mega-meteoritic dangers. A close-up study will also decrease the uncertainty of the moonlet's orbital period about Didymos, the primary, where current uncertainties are limited by the precision of measurements taken from ground observatories. The crater shape will finally be known, as well as the moonlet's mass. Hera is set for launch in October 2024, with a planned arrival at Dimorphos in December 2026 [14].

Gravimetry

In addition to observing the impact crater, Hera will measure the mass of Didymos' small companion. Dimorphos, the main subject of the study, will be the smallest asteroid visited so far, with Hera's planned launch of 2024 and arrival 4 years after DART [3]; [14]. As previously mentioned, the estimated combined mass of the Didymos system is 5.28×10^{11} kg [28].
The Gravimeter for Small Solar system bodies (GRASS) gravimeter is designed to measure gravitational variations in the self-gravity of small bodies, such as Mars' moon Phobos, for the Martian Moons eXploration (MMX) mission by Japanese Aerospace Exploration Agency (JAXA). For Hera en route to Didymos and its moonlet Dimorphos, the GRASS instrument will be miniaturised and placed on the Juventas CubeSat. A prototype of the gravimeter was developed by ROB together with EMXYS from Spain. It will be the first gravimeter that will land on a small body in history, with another example of a gravimeter in space being on our Moon. The design chosen by ROB is a relative gravimeter, meaning it measures the variations in gravitational acceleration based on a reference point and it should have an accuracy better than a millionth of Earth's gravity. The Juventas cubeSat will slowly fall onto Dimorphos, with GRASS recording the gravitational variations during the fall, impact and subsequent bounces on the surface ([12, 19], Tasev 2019 [32]) .
Sending a gravimeter with Hera will mean that information about the exact mass of the moonlet will finally be known, subsurface density information can be collected, mass anomalies due to porosities in the rock for example, can be measured and researchers can learn about the mass distribution on the moonlet Dimorphos. The local composition can also be deduced when combining the density information with e.g. spectra. Over longer periods, possible variations due to tidal interactions with Didymos can also be recorded [19, 32].

1.4 Thesis Goals

When I started my master's thesis, a few goals were suggested by my supervisors and me. Dr Senel and I had an in-depth meeting where we discussed certain ideas of what we could do that would be both useful to ROB and Dr Karatekin's team, as well as interesting and informative for me as a student.
The reason for this discussion was to narrow down the scope of the research, as the thesis topic proposal was quite broad (see Appendix A.1), including many different avenues. In addition to the vast topic, the realistic amount of time I could dedicate to my thesis meant that the project's scope had to be decreased to a manageable level in order to produce anything useful.

Scientific Goals

The scientific goals relate to what results we wished to gain from this study. The main idea was to constrain or uncover different possibilities of Dimorphos' parameters with regards to the DART impact crater. Briefly, we wanted to get:

- A range of the different possible crater shapes on Dimorphos given the known DART impact parameters,
- Dimorphos's self-gravity given the different crater morphologies obtained,
- The magnitude of gravity anomalies on post-impact Dimorphos due to the cratering.

Didactic Goals

After I got into contact with the promoters for this master thesis topic and bearing in mind that it was not at the University of Liège, but at ROB, I had some personal goals relating to what I wanted to learn from the experience, as well as skills I desired to develop.
My goals were to:

- Learn the shock-modelling programmes of *iSALE2D* and the smooth particle hydrodynamics (SPH),
- Learn about asteroid craterisation and impacts on solar system bodies, including crater morphologies, momentum transfer and ejecta dynamics,
- Expand and apply my knowledge from my courses, namely on the topic of small bodies of the solar system,
- Expand my knowledge of the DART mission and the European contributions to it,

- Expand my knowledge of shock physics and fluid dynamics,
- Practice implementing and modifying post-processing scripts in Python.

2 Theoretical Background

2.1 Physical Parameters

Strength Cohesion

The strength or cohesion of a body is a measure of how resistant the material is to damage or how easily it can break up. There are different types of strengths, such as yield strength, material strength, shear strength and tensile strength. Small bodies with iron-nickel cores for example are more resistant to disruption and can survive more collisions than other bodies, such as rubble piles. Below a certain strength value, the small body is held together solely by its self-gravity ([9] p385-387).
The strength regime on Dimorphos is thought to be greater than ~ 3.5 Pa. Below this threshold, the impact becomes gravity-dominated, meaning gravity dominates over the strength of the material, usually resulting in larger craters. [3, 15].

Porosity

The porosity refers to how much empty space is within the asteroid. Low porosity means the material is quite coherent, with very few empty spaces. This might be the case for an M-type asteroid. A high porosity suggests the asteroid is a rubble pile, with lots of different sizes of rocks and boulders agglomerating into a gravitationally bound body with lots of void spaces.
Porous materials have a pressure as a function of ρ bulk density, E internal energy and α distension. Distension is the ratio of the density of the solid material ρ_s to the bulk density ρ, i.e. $\alpha = \rho_s/\rho$. Porosity ϕ, is

$$\phi = 1 - \frac{1}{\alpha}$$

In iSALE-Dellen the input for porosity is the distension $\alpha = \frac{1}{1-\phi}$ (see Section 3) ([5] p85).
ON THE PARAMETERS
It is useful to categorise or sort asteroids using the two parameters of strength and porosity as they help determine the body's reaction to impacts. High cohesion and low porosity suggest a monolithic object, i.e. a coherent body, which could be moderately fractured. These objects might develop fractures after a collision. Medium strength cohesion and low porosity suggest a highly fractured object. These would be harder to break apart due to the fractures inhibiting the

propagation of impact waves. Finally, our rubble piles are characterised by low strength and medium to high porosity. The impact energy in rubble piles would be damped quickly and craters would form from the compaction of material under the impact (Planetary Sciences [9] p387).
We can assume that larger bodies would be covered in a layer of regolith, as meteoroids and micrometeoroids would pulverise the surface rock over time. This is what can be seen on the Moon. Dimorphos is not in this size category, however. So we can assume this rubble pile's regolith would be mixed up with other debris of varying size and behave much differently than lunar regolith [25].
Crater morphology is expected to depend on these parameters. In the cohesion range of 0–18 MPa, crater diameters are expected to decrease with an increase in cohesion [31]. In the porosity range of 0–50%, the ratio between crater depth and crater diameter tends to increase above $\sim 30\%$, staying approximately constant in the 0–30% range [31].

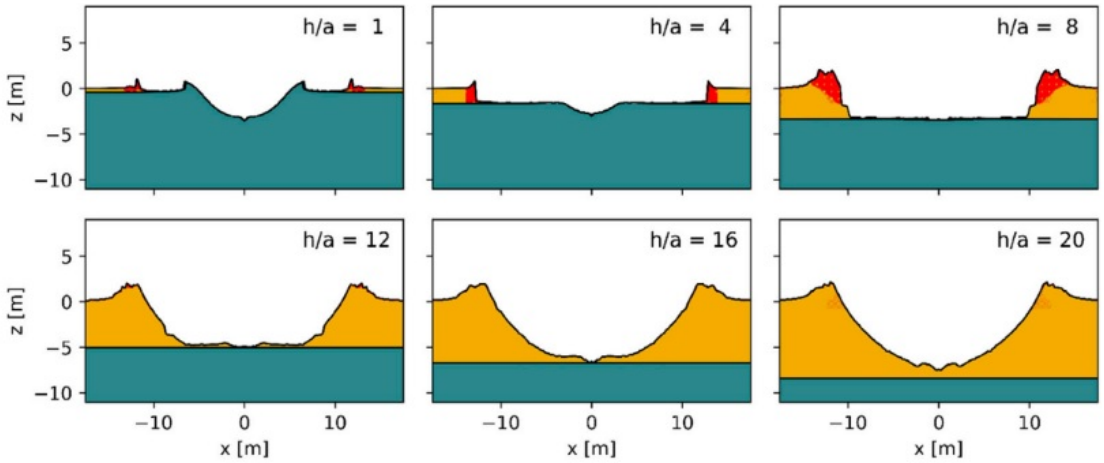

Figure 2: Crater geometries: $h/a = 1$ concentric crater,$h/a = 8$ flat-bottomed, $h/a = 12$ central-mound, $h/a = 20$ bowl-shaped/normal. h is the regolith thickness and a is the impactor radius. Taken from Figure 5 in Raducan et al. 2020 [25]

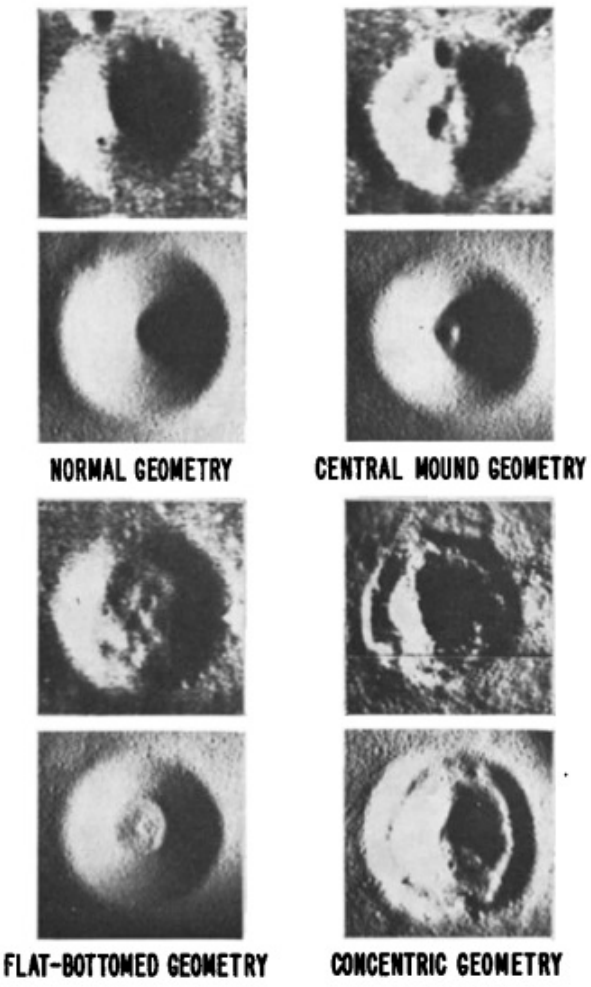

Figure 3: Lunar (top) and laboratory (bottom) crater geometries. Taken from Fig. 1 in Quaide & Oberbeck 1968 [24]

Crater morphology can also be described by its shape or geometry. The 4 main types identified by Quaide & Oberbeck are the normal, flat-bottom, concentric and central-mound craters, as illustrated in Figs 2, 3 [24, 25].

2.2 Gravity Anomaly

Simply put, in geophysics, gravity anomalies are the difference between the gravity measured at a point and the predicted value of gravity at that point in a reference ellipsoid. Certain corrections have to be applied to it to account for different features that will affect gravity, namely elevation and mass of the surrounding rock, among other factors.
The reference ellipsoid is a spheroid that best fits the shape of the Earth. The geoid is a smooth surface that approximates the mean sea level on Earth.

The anomalous gravity can be estimated using the following equation

$$\Delta g = g_P - \gamma_P = g_P - (\gamma - \delta g_F + \delta g_B - \delta g_T)$$

Here we have Δg as the gravity anomaly, g_P is the gravity measured at a specific point named P, and γ_P is the model value of gravity at the particular point P. γ_P itself takes various factors that influence gravity into account:

$$\gamma_P = \gamma - \delta g_F + \delta g_B - \delta g_T$$

Here, γ is the acceleration due to gravity on the surface of the reference ellipsoid, known as normal gravity. It accounts for the Earth's mass and rotation.
δg_F is called the free-air correction, which will be defined shortly, along with δg_B, the Bouguer correction. Finally, we have δg_T, called the terrain correction, taking the effects of the rugged and non-smooth terrain into account (Encylopedia of Solid Earth Geophysics p524-533 [13]).

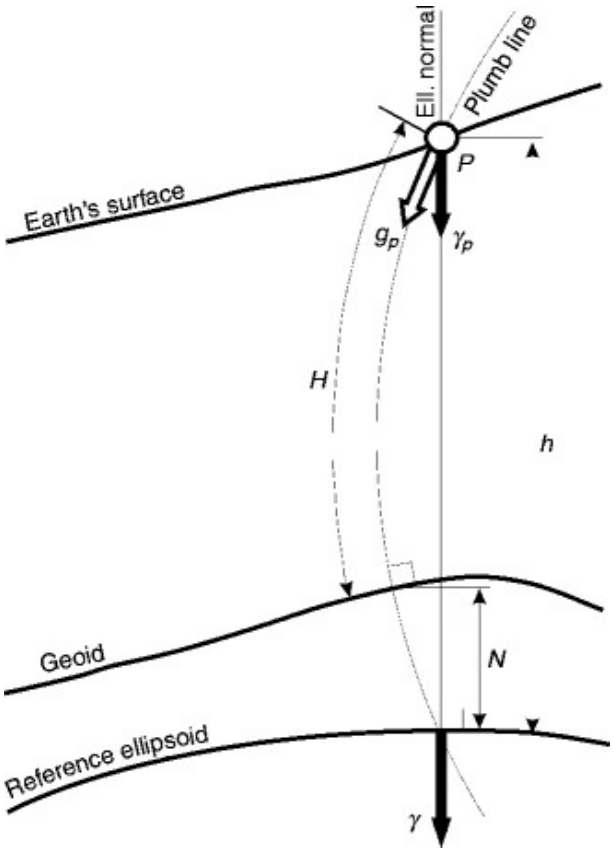

Figure 4: From Figure 1 of "Gravity, Data to Anomalies" *Encylopedia of Solid Earth Geophysics*, p524-533 [13]

Free-air correction

The free-air correction δg_F accounts for the gravity effects of a difference in elevation between the reference ellipsoid and the point of measurement. Gravity decreases proportionally to the square of the distance, $a \propto 1/r^2$. The free-air correction is computed from the height h of the measured point P above the reference ellipsoid (see Fig. 4) [13].

Bouguer correction

The Bouguer correction δg_B is named after the French physicist Pierre Bouguer. It accounts for the mass of rock between the measured point and the reference ellipsoid. The rock evidently will have a mass, therefore affecting the gravity measured at point P. To account for this rock, geophysicists usually make approximations of the form of an infinite flat rock slab of thickness equal to the ellipsoidal height h, or a spherical cap of thickness h, accounting for the curvature of the Earth. Fig. 5d illustrates the approximation of an infinite slab above the reference ellipsoid [13].

Terrain correction

Other corrections exist, such as the previously mentioned one accounting for the topography of the area, called the terrain correction δg_T. The ruggedness matters because the Bouguer correction assumes a smooth surface in the form of the infinite slab or the spherical cap. By subtracting gravity from the mass that was assumed to fill empty areas (because less mass below means less gravity at P), as well as subtracting gravity from the mass that is above (because more mass above means less gravity at P) the measured point, ruggedness is corrected from the Bouguer anomaly. Fig. 5e illustrates how the terrain correction differs from the Bouguer correction in Fig. 5d [13].

mGal units

The commonly used and accepted unit for gravity is not the standard SI unit of m s^{-2} but rather the mGals (milligals). The name comes from Galileo Galilei and is defined as 1 mGal = 10^{-5}m s^{-2} in the standard SI mks unit base. [13]
Nota bene
These definitions come from geophysics and are strongly grounded in an Earth-centric view and context. The concepts can apply to asteroids, but we must be wary that there are no standards on Dimorphos. For example, the reference ellipsoid or the rock mass on Earth is all set to agreed-upon values, which is not the case for Dimorphos.

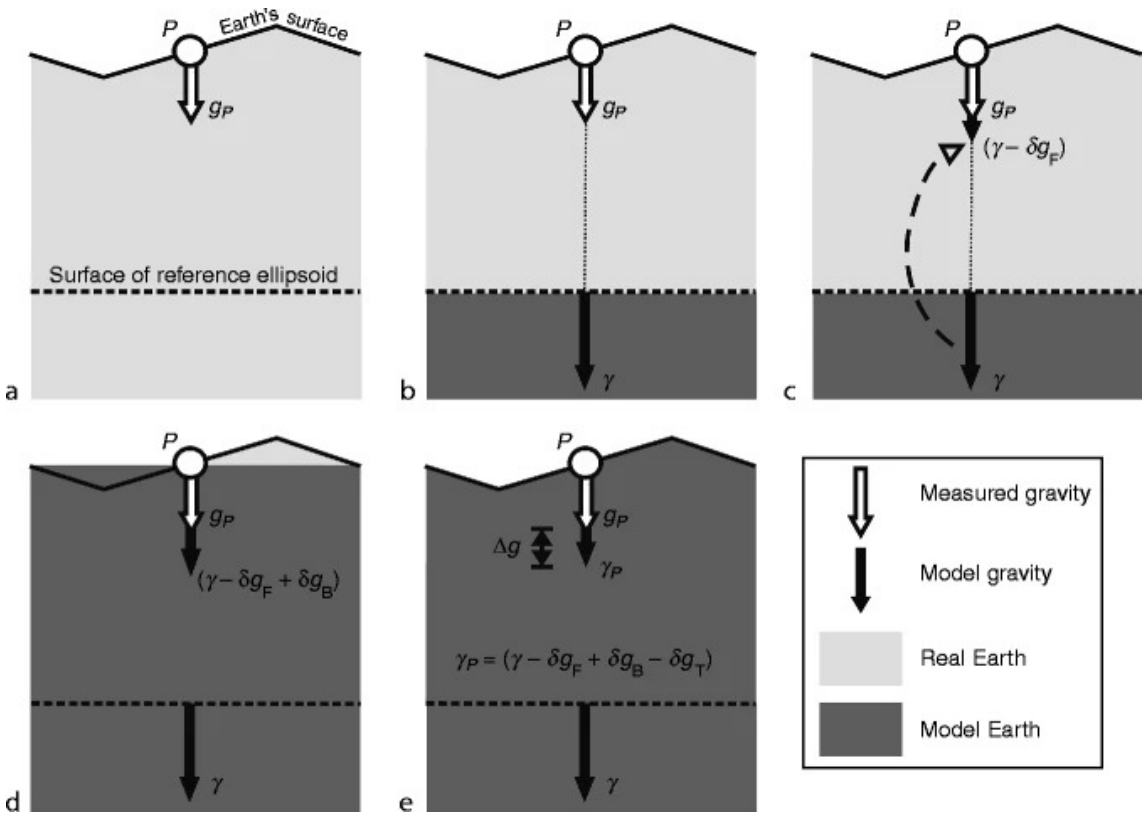

Figure 5: From figure 2 of "Gravity, Data to Anomalies" *Encylopedia of Solid Earth Geophysics* , p524-533 [13]

3 Methodology

This master thesis combines different works to form a story of Dimorphos and its DART-created crater, from the two-dimensional hypervelocity shock physics impact simulations in iSALE-Dellen to the gravitational potential calculations with Ms Tasev's polyhedron gravity model script.
The greatest chunk of the work was by far the setting up and handling of the two-dimensional shock physics impact simulations. My supervisor, Dr Senel set up a few example cases for me to adjust according to our agreed-upon scenarios for the impact crater.
Although smaller in proportion, the next part was equally as important, as it involved the gravitational computations in collaboration with Ms Tasev at ROB. She very kindly converted the 2D impact craters simulated in the previous section into full three-dimensional shape models, which I then used to compute the gravitational potential on Dimorphos post-impact using her script.

2D impact crater simulations cohesion and porosity values		
Porosity ϕ	Strength Y	Reference Figure
10%	1 kPa	11a
10%	10 kPa	10a
10%	100 kPa	9a
30%	1 kPa	11b
30%	10 kPa	10b
30%	100 kPa	9b
50%	1 kPa	11c
50%	10 kPa	10c
50%	100 kPa	9c

Table 2: *iSALE2D* impact crater simulation constant parameters and the resulting simulation plots.

Luther et al. 2D DART impact craters		
Porosity ϕ	Strength Y	Reference Figure
10%	1 kPa	6a
10%	10 kPa	7a
10%	100 kPa	8a
50%	1 kPa	6b
50%	10 kPa	7b
50%	100 kPa	8b

Table 3: Luther et al. *iSALE2D* impact crater simulations. Provided by Luther et al. 2022 from private correspondence [22]. The resulting 3D shape models can be found in Appendix A.4

3.1 DART Parameters

From DART's 26 September 2022 impact, several parameters are already known. This information was taken into account and used in the models. Table 4 summarises all the relevant parameters needed on Dimorphos and the DART impact. Some of the details are based on studies of Dimorphos and DART, but others are approximations adopted in similar simulation studies (Raducan et al. 2022 [26]; Senel et al. 2023 [30]).

DART Parameters		Reference
DART mass	> 300 kg	[2]
	310 kg	[25]
	650 kg	[26, 30]
DART density	1000 kg m^{-3}	[25]
DART diameter	1 m	[2]
	0.84 m	[25]
DART impact velocity	6.67 —7.38 km s^{-1}	[2]
	7 km s^{-1}	[25]
	6.5 km s^{-1}	[30]
	6.145 km s^{-1}	[3]
DART impact angle	27.5°	[2]
Binary system mass	5.28×10^{11} kg	[28]
	$5.4 \pm 0.4 \times 10^{11}$ kg	[17]
Binary system density	2400 kg m^{-3}	[4]
	2170 ± 350 kg m^{-3}	[17]
Didymos density	2.146(±30%)g cm^{-3}	[2]
Dimorphos mass	4.8×10^{9} kg	[28]
Dimorphos density	1500–3300 kg m^{-3}	[4]
Dimorphos porosity	0–50 %	[16]
Dimorphos yield strength	> 3.5 Pa	[3]

Table 4: Main DART parameters from literature and other simulations.

3.2 iSALE-Dellen

The release version of the iSALE code used for the majority of my work is called iSALE-Dellen (Collins et al. 2016 [5]) and is an improvement on the SALE shock physics hydrocode developed in 1980 (Amsden et al. 1980 [1]). The "i" in iSALE stands for "impact" and the modifications allowing hypervelocity impact simulations were developed in the 1990s (Ivanov et al. 1997 [20], Melosh et al. 1992 [23]). In 2004, the strength model was modified (Collins et al. 2004 [6]), the porous compaction $\epsilon - \alpha$ model was added in 2006 (Wünnemann et al. 2006 [33], Collins et al. 2011 [7]), a 3D version was implemented in 2009 (Elbeshausen et al. 2009 [10]), and the dilatancy model 5 years later (Collins 2014 [8]).
The iSALE repository is held at the Museum für Naturkunde in Berlin, Germany. It is used extensively in the study of impact craters, especially lunar and terrestrial ones. The developers and contributors, who are formally acknowledged in Section 5, distribute iSALE hydrocode on a case-by-case basis.
Dr Senel was already familiar with this program and helped me set up the different cases we were going to simulate. We decided to have 9 different cases separated into 3 different levels of constant cohesion and 3 different levels of constant

porosity, following the paper by Luther et al. 2022 and Raducan et al. 2022. Refer to Table 2 for a list of the 9 cases and their corresponding constant parameter. The setup files that include the different parameters for each of the 9 cases can be found in Appendix A.5. The main parameters I had to be wary of and modify based on the case, were the target's strength, porosity and the simulation stop time. This stop time was important to allow enough time for the crater shape to settle into its final form. If the time was set to stop too early, the crater would still have changed significantly afterwards had the simulation been left running (see Appendix A.2). If the time was set up too late, the computation time would be immense with little to no new useful information about the crater morphology. In the end, I set most of the simulations to finish at 6 seconds, while monitoring the crater evolution throughout. If I assessed that the crater had evolved into its final shape and size and was not going to change further given more time, then I would cut the simulation short.

Description	Value
Thickness of lithosphere	100 m
Radius of planet	80 m
Gravitational acceleration	-5×10^{-5} m s^{-2}
Number of layers	1
Projectile parameters	
Object velocity	-6.5×10^{3} m s^{-1}
Object type	spheroid
Time parameters	
Initial time increment	2×10^{-3} s
Maximum timestep	0.1 s
End time	0.5–7.5 s
Save interval	0.04 s

Table 5: Model parameters for the iSALE2D simulations

Single-layer 2D Scenario

Description	Target	Impactor
Material	Basalt	Aluminium
Equation of state	Tillotson	Tillotson
Strength model	Lundborg	Johnson-Cook
Dilatancy model	ALPHAPT	none
Damage model	none	none
Acoustic fluidisation	none	none
Porosity model	Wünnemann	none
Elastic strength poisson ratio	0.25	0.33
Lundborg strength parameters		
Cohesion Y_0	$1e3$, $1e4$, $1e5$	none
Internal friction coeff. μ	0.77	none
High pressure lim. strength Y_m	$1e9$	none
Johnson-Cook strength parameters		
Strain coeff. A	none	$2.44e7$
Strain coeff. B	none	$4.88e7$
Strain exponent n	none	0.5
Strain rate coeff. C	none	0.02
Thermal softening m	none	1.7
Reference temperature	none	$2.93e2$
Wünnemann porosity parameters		
Initial distension α_0	1.111, 1.429, 2.0	none
Elastic volumetric strain threshold ϵ_{e0}	-2×10^{-8}	none
Distension transition α_x	1.05, 1.1, 1.15	none
Exponential compaction rate coeff. κ	0.76, 0.97, 0.98	none
Material sound speed ratio χ	0.8, 0.3, 0.3	none

Table 6: Material parameters for the iSALE2D simulations.

The Tillotson equation of state (EoS) is designed by J.H. Tillotson in 1962 for high-velocity impact computations (please refer to the iSALE manual [5] p78-81) and it was used in previous simulation studies in iSALE focussing on DART and Dimorphos [25, 26, 22, 30], whereas lunar cratering simulations in iSALE used another EoS[21]. Different EoS are sometimes used in other hydrocodes as well [31].
The dilatancy model ALPHAPT is defined with the equation:

$$\beta = \beta_{max} \left(\frac{\alpha_c - \alpha}{\alpha_c - \alpha_{min}} \right) \left[1 - \frac{\log(p/10^5)}{\log(p_{lim}/10^5)} \right] \tanh \left\{ \xi \left(\frac{T}{T_m} - 1 \right) \right\}$$

The Lundborg strength model defines the yield strength Y to depend on pressure p, cohesion Y_0 (which is the same as the yield strength at zero pressure), the

coefficient of internal friction of the material μ and the limiting strength at high pressures Y_m, which are called YDAM0, FRICDAM and YLIMDAM respectfully in the asteroid setup file (see Appendix A.5). This leaves us with the equation:

$$Y = Y_0 + \frac{\mu p}{1 + \frac{\mu p}{Y_m \breve{} Y_0}}$$

The model is denoted as LUNDD in the iSALE files ([5] p88).
The Johnson-Cook strength model for metals, a.k.a. JNCK in the files, is defined as

$$Y = \left(A + B\epsilon^N\right)\left(1 + C\ln(\dot{\epsilon})\right)\left[1 - \left(\frac{T - T_{ref}}{T_m \breve{} T_{ref}}\right)^M\right]$$

If we ignore the temperature dependence (m =none), we can simplify the relation by eliminating the part in square brackets. Our parameters here are the equivalent plastic strain ϵ, the strain rate $\dot{\epsilon}$, the temperature T and the rest are parameters as defined in Table 6. They are JC_A, JC_B, JC_C, JC_N, JC_M, JC_TREF in the material.inp files (see Appendix A.5). The projectile impactor follows the JNCK strength model for Aluminium. It has no porosity, no dilatancy, no acoustic fluidisation nor any damage model ([5] p89, 116).
The porosity model we used is the Wünnemann porosity model.

Distension from Porosity		
Low	10%	α_0 =1.111
Medium	30%	α_0 =1.429
High	50%	α_0 =2.000

Table 7: Distension inputs $\alpha_0 = [1 - \phi]^{-1}$ from porosity levels for *iSALE2D* simulations [5]

The input parameters in the material setup file (see Appendix A.5) are: α_0 as the initial distension of the porous material, which is the inverse of $1 - \phi$ (see Section 2.1),

$$\alpha = \frac{1}{1 - \phi}$$

where ϕ is our porosity fraction or percentage, ϵ_{e0} is the elastic volumetric strain threshold, α_x is the distension at the transition from an exponential to a power-law compaction regime, κ is the compaction rate parameter in the exponential regime and χ is the ratio of porous material to solid material sound speed at a pressure of 0. The respective names of these parameters in the input files are ALPHA0, EPSE0, ALPHAX, KAPPA and CHI ([5] p85-87).
Recall that we have 3 different constant porosities in our 9 cases: low porosity, which we set as 10%, medium porosity 30% and high porosity 50%. This means

that for our simulation cases, the porosities as determined by the distension α_0 as portrayed in Table 7:

$$\phi = 10\% \rightarrow \alpha_0 = \frac{1}{1-0.1} = \frac{1}{0.9} = 1.111$$

$$\phi = 30\% \rightarrow \alpha_0 = \frac{1}{1-0.3} = \frac{1}{0.7} = 1.429$$

$$\phi = 50\% \rightarrow \alpha_0 = \frac{1}{1-0.5} = \frac{1}{0.5} = 2.000$$

Table 5 shows some of the parameters of the simulation setup. The end times for the simulation varied from case to case, depending on the evolution of the impact crater for the given parameters of cohesion and porosity, as will be explained in Section 4. Initially, the high cohesion cases were set to 0.5 s but were changed when I noticed some required more time. The low cohesion cases were initially set to end after 6.0 s, as that was seen as enough time for the crater to settle into its final depth and diameter.

3.3 pySALEPlot

The *iSALE2D* program in iSALE-Dellen does not include any post-processing capabilities or data visualisation tools itself. The developers do, however, offer a Python library of scripts and functions that take care of plotting needs, called *pySALEPlot*.

Post-processing

My supervisor, Dr Senel, shared some Python scripts with me that he had used in previous studies [29, 30], which I modified according to my needs and preferences. In Appendix A.5, the output fields are denoted as #Den-Tmp-Pre-Sie-Yld-Alp-TPS-Yac-VEL#. These are the variables that are returned by iSALE2D after a simulation run. We can then use these to plot the data as we wish.
I used the distension #Alp and the density #Den to plot the porosity and density of the crater at certain simulation times, mainly at the end of the simulation. This was to see what the craters looked like at the point where I expected them to not change anymore.
pySALEPlot includes some built-in functions to call onto the model data, such as for calculating the gravity anomalies. I had the option to plot both the Bouguer anomaly and the Free-air anomaly for the crater, using different calculation methods, depending on if I wanted to use the distension or the density outputs.
As mentioned before, I had to plot the crater evolution throughout the simulation to see if the chosen end time was appropriate. To do this I could plot the crater

radius and crater depth over simulation time. Theoretically, if the crater stopped increasing in depth and in diameter for a few milliseconds (roughly 100–200 ms), the final shape had been reached. We will later see a case where waiting a bit longer was beneficial as the crater shrunk, so it was important to give the simulation enough time for the crater to settle itself.

3.4 Polyhedron Gravity Model

Ms Elisa Tasev programmed a gravitation model called the Polyhedron gravity model (PGM) during her master thesis in 2019 at the ROB. This model uses the constant density polyhedron method and is specialised in evaluating the gravitation of non-spherical bodies, more precisely, irregularly-shaped small bodies such as asteroids and comets. It is implemented in Matlab R2017a as a script (Tasev 2019 [32]).
The goal of her script is to be able to measure the gravity fields of different small bodies that are inputted as three-dimensional shape models. The gravity information can then be visualised in a publically available 3D program called the Small Body Mapping Tool (SBMT), developed at the Johns Hopkins Applied Physics Laboratory in Maryland, USA. This program allows users to project asteroid or comet data from various spacecraft onto 3D shape models of these small bodies [11]. In our case, we project the calculated potential gravity of Dimorphos resulting from the impact crater.
Ms Tasev showed me how to use the SBMT in tandem with her script. Here are the steps we took to get our results:

- First, we obtain the two-dimensional iSALE impact crater morphologies for our case, e.g. a porosity of 30% and a cohesion of 10 kPa.
- Using the 3D modelling software known as *Blender*, Ms Tasev creates a shape model of the Dimorphos impact crater based on the previous simulations, which she then shares with me.
- The polyhedron gravity modelling script reads the 3D shape model of Dimorphos with the impact crater as an object ".obj" file.
- The script computes the gravitational potential and outputs it the results in a text ".txt" file.
- The same Dimorphos shape model with the appropriate impact crater for the case is imported into the SBMT software.
- The gravitational potential information for that particular shape model is inputted as "Plate colouring data" in SBMT.

- After some adjusting, the result is a colour-coded three-dimensional model of Dimorphos with the impact crater at the specific porosity and cohesion case.

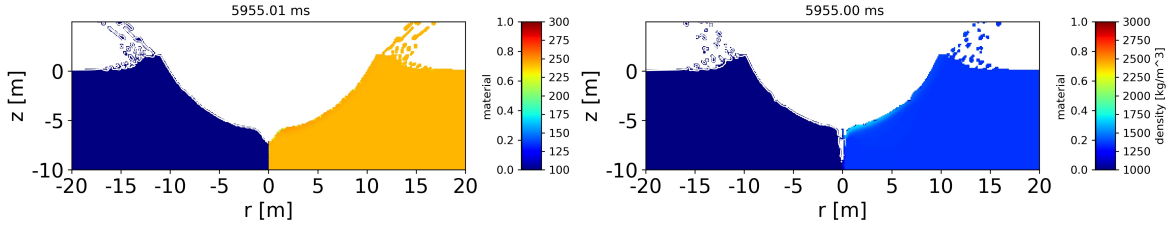

(a) $Y_{d0} = 1$ kPa, $\phi = 10\%$ at 5955 ms (b) $Y_{d0} = 1$ kPa, $\phi = 50\%$ at 5955 ms

Figure 6: 1 kPa cases courtesy of Robert Luther and co-authors [22]

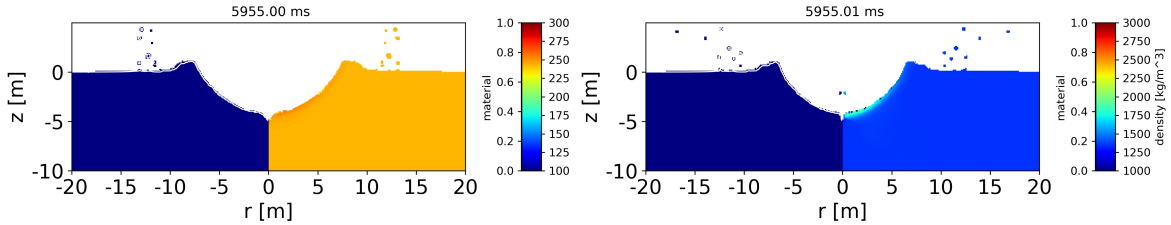

(a) $Y_{d0} = 10$ kPa, $\phi = 10\%$ at 5955 ms (b) $Y_{d0} = 10$ kPa, $\phi = 50\%$ at 5955 ms

Figure 7: 10 kPa cases courtesy of Robert Luther and co-authors [22]

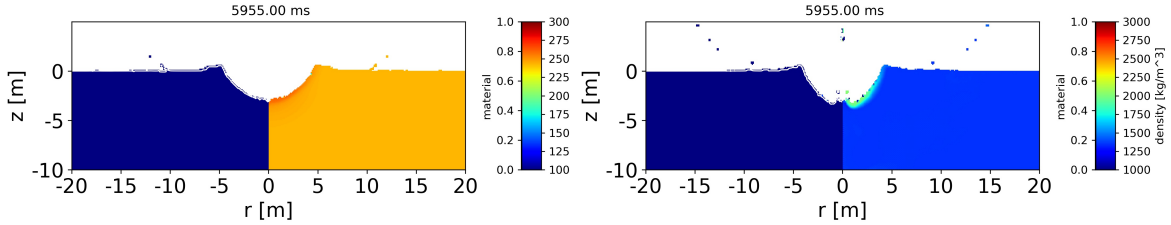

(a) $Y_{d0} = 100$ kPa, $\phi = 10\%$ at 5955 ms (b) $Y_{d0} = 100$ kPa, $\phi = 50\%$ at 5955 ms

Figure 8: 100 kPa cases courtesy of Robert Luther and co-authors [22]

Nota Bene
Many of the Blender-made shape models from Ms Tasev are based on the figures kindly shared with us by Dr Robert Luther from the Luther et al. 2022 paper [22].

This was a preliminary test of the method. For a list of the parameters and the resulting plots used by these, please see Table 3. My simulations (see Table 2) use almost the same scenarios as the Luther et al. paper, except for a porosity of 30%, for which Ms Tasev also made 3D shape models.
On another note, the three-dimensional shape models made in Blender are all essentially bowl-shaped i.e. they have a normal geometry according to the designations in Raducan et al. 2020 and Quaide & Oberbeck [25, 24]. The essential features modelled are the crater diameter and depth, including the ridge along the circumference. This means the individual geometry of the craters is not modelled exactly.

4 Results & Discussion

4.1 2D Simulations

As highlighted in Appendix A.2, I ran a first round of simulations in iSALE for a range of porosities and strength cohesions for a simulated time of 100 ms. As mentioned in Section 3, the porosities were separated into 3 cases: low porosity of 10%, medium porosity of 30% and a highly porous 50%. The cohesion was likewise distributed into 3 groups: high cohesion of 100 kPa, medium cohesion of 10 kPa and a low cohesion of 1 kPa. Together we have the 9 cases (see Table 2).
The problem encountered was that 100 ms was not enough for the crater morphologies to settle into their final form; more time had to be given for the crater to settle properly. This is evident in the crater evolution plots, showing crater diameter and crater depth evolution over simulation time. I restarted the simulations with the added condition that I check that the craters settle into their final forms. This was decided when both the diameter and depth did not change for a few hundred milliseconds, or when both curves stop increasing and reached a plateau on the crater evolution plots.

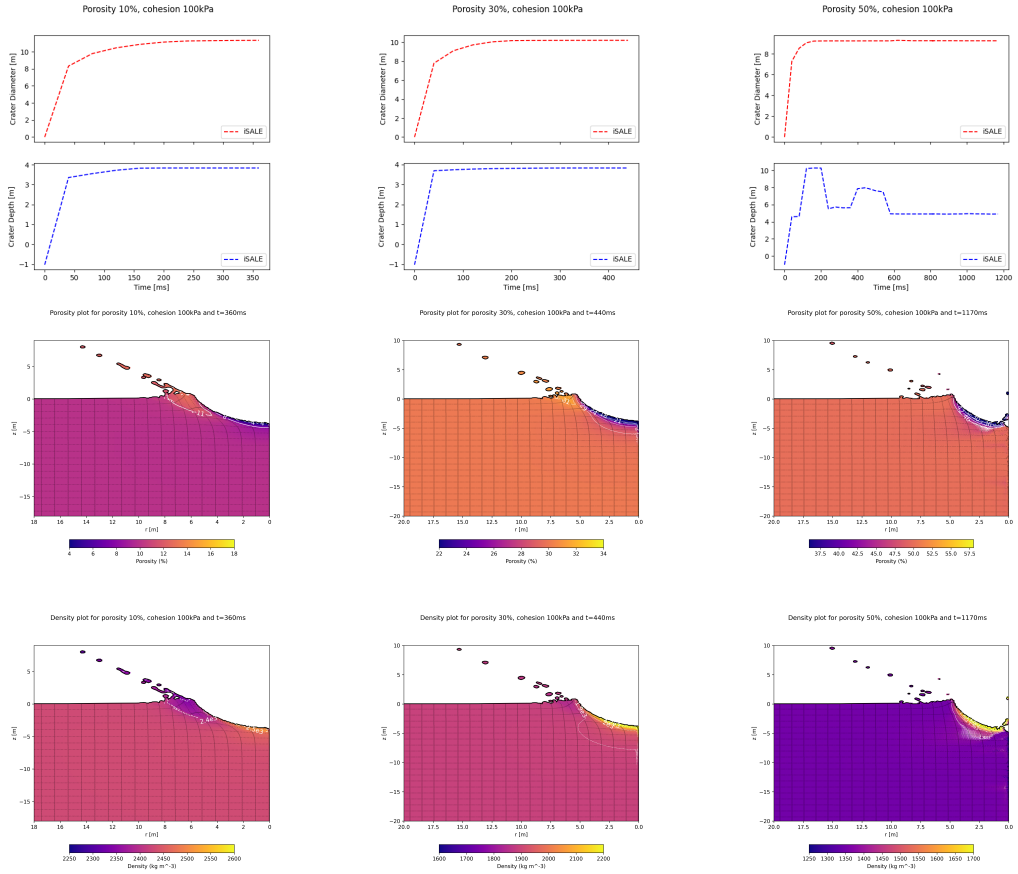

(a) $\phi = 10\%$ $Y_{d0} = 100$ kPa at 360 ms (b) $\phi = 30\%$ $Y_{d0} = 100$ at 440 ms (c) $\phi = 50\%$ $Y_{d0} = 100$ kPa at 1170 ms

Figure 9: 100 kPa crater evolution and contour plots of porosity and density

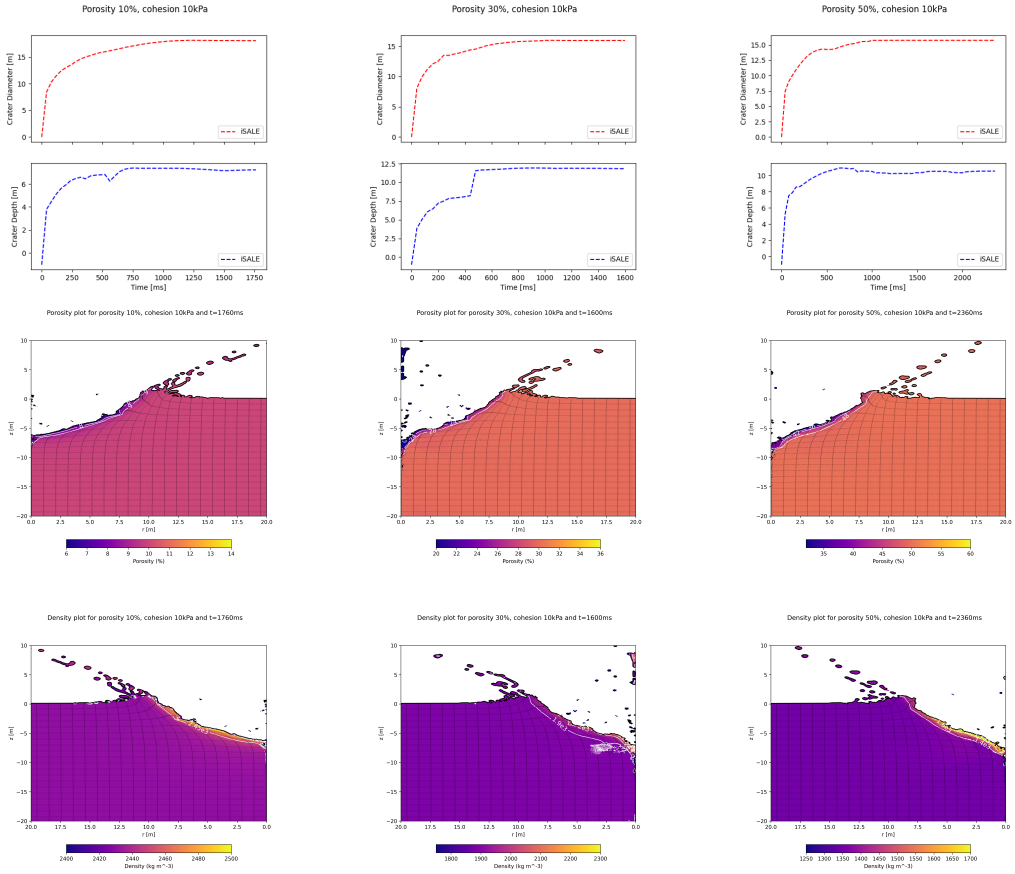

(a) $\phi = 10\%$ $Y_{d0} = 10$ kPa at 1760 ms (b) $\phi = 30\%$ $Y_{d0} = 10$ kPa at 1600 ms (c) $\phi = 50\%$ $Y_{d0} = 10$ kPa at 2360 ms

Figure 10: 10 kPa crater evolution and contour plots of porosity and density

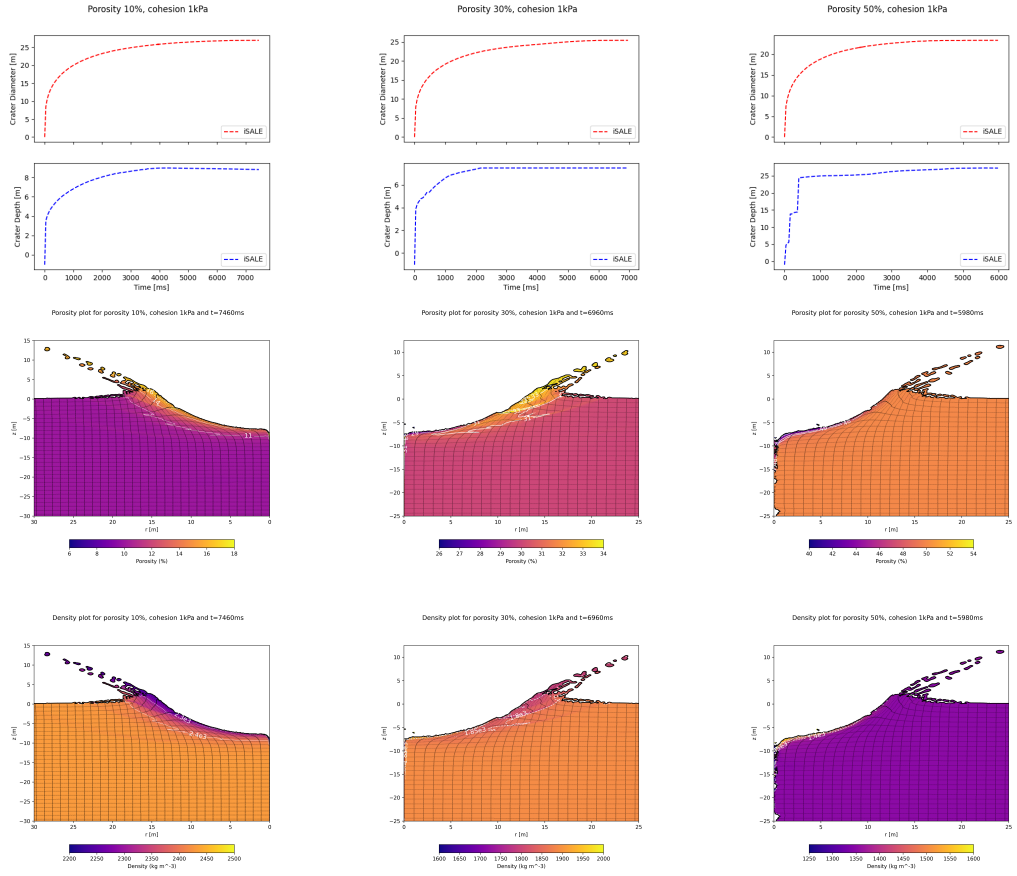

(a) $\phi = 10\%$ $Y_{d0} = 1$ kPa at 7460 ms (b) $\phi = 30\%$ $Y_{d0} = 1$ kPa at 6960 ms (c) $\phi = 50\%$ $Y_{d0} = 1$ kPa at 5980 ms

Figure 11: 1 kPa crater evolution and contour plots of porosity and density

The plateaus are evident in the crater evolution figures. We could thus hypothesise that running the simulations for a few days longer would not change the crater shape significantly.
Figure 9c showing the case of 100 kPa cohesion at 50% porosity has a remarkably unique crater evolution curve when it comes to depth. We can see it increases in depth quite fast but decreases at around 200 ms, only to increase and decrease again 200 ms and 400 ms later respectively. It seems to be the case that this was caused by either ejected material coming back down into the crater and filling it up slightly, or that the central mound, which is barely visible, is contributing to these abrupt changes.
If we visualise the density profiles over some time, we can see the crater evolution and the central mound breaking off (Figures 27,28).
We can see in some figures that the porosity increased and the density decreased after impact. For example, at low cohesion of 1 kPa, Fig. 11c follows the trend of

the higher cohesions where the impact site has a lower porosity than the pre-impact area, whereas for Figures 11a and 11b the porosity increases by a few per cent at the impact crater site.
The crater sizes are also worth looking over. The crater diameter gets smaller with increasing cohesion, which is consistent with Stickle et al. 2022 (Table 1 of [31]). We can also see a very slight dependence on crater diameter with porosity, where a higher porosity leads to a slightly smaller diameter. This is also consistent with Stickle et al. 2022 [31]. We are supposed to also see the ratio between crater depth and diameter increase above a porosity of 30% according to Stickle et al. This is the case for my 1 kPa craters, as the $\frac{\text{depth}}{\text{diameter}}$ ratio visibly increases at 50% porosity when compared to the 30% and 10% cases. However, this trend of the ratio increasing above 30% is not visible in the medium and higher cohesion cases.
We can analyse the crater morphologies according to shapes such as in Quaide & Oberbeck 1968 and Raducan et al. 2020, where they highlight the 4 different crater geometries: normal or bowl-shaped crater, concentric crater, central mound crater and flat-bottom crater (see Figs 2 3) [24, 25]. Most of the contour plots show clear bowl-shaped geometries for our simulations. Some craters show a central-mound geometry, notably ...

Gravity Anomalies

We saw in Section 3.3 that pySALEPlot contains functions to plot the Bouguer anomaly and the free-air anomaly. Figures 15,16,17 show the density and porosity contour plots with the Bouguer anomaly plotted above. The values of the anomalies differ depending on whether the plot displays the density or the porosity (recall that they are related to one another through the distension). It appears this is because the anomaly calculation functions by pySALEPlot have the option to include the output variables of density or porosity, meaning the computations of the anomaly is different. The reference density used in the pySALEPlot scripts was 2700 kg m^{-3} with an altitude of 0.0 m.

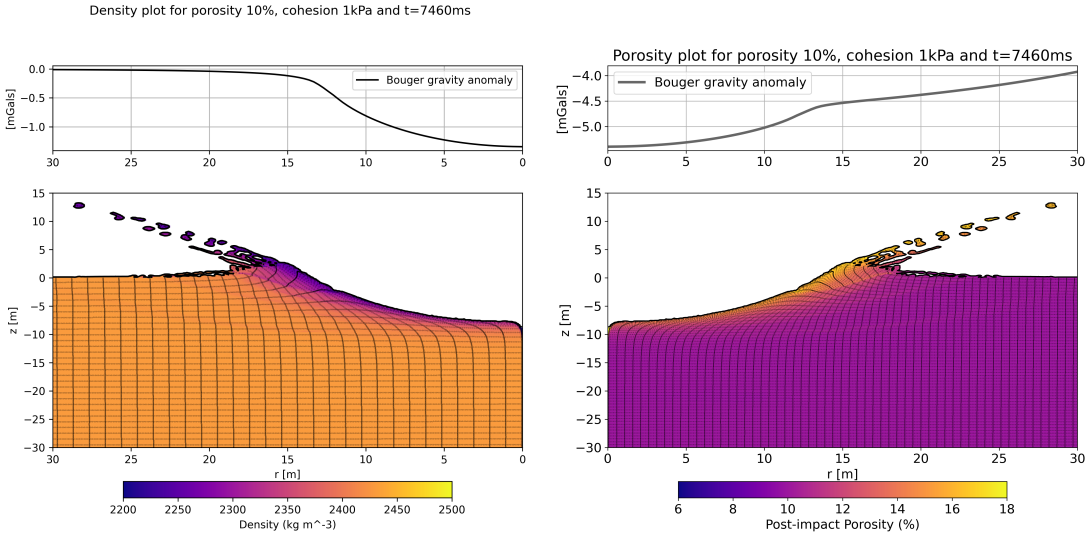

(a) Density (b) Porosity

Figure 12: Bouguer anomalies for 10% 1 kPa case

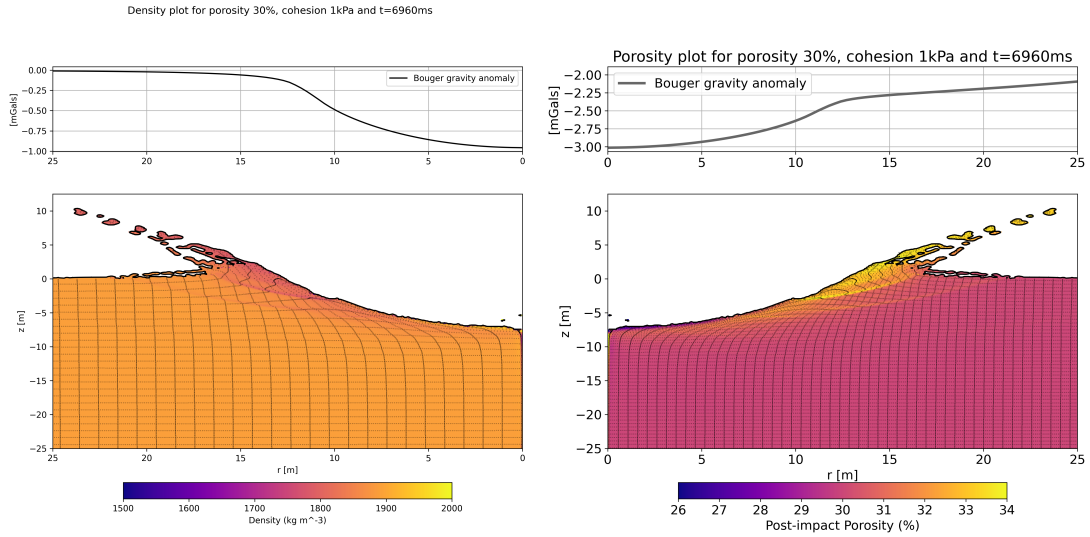

(a) Density (b) Porosity

Figure 13: Bouguer anomalies for 30% 1 kPa case

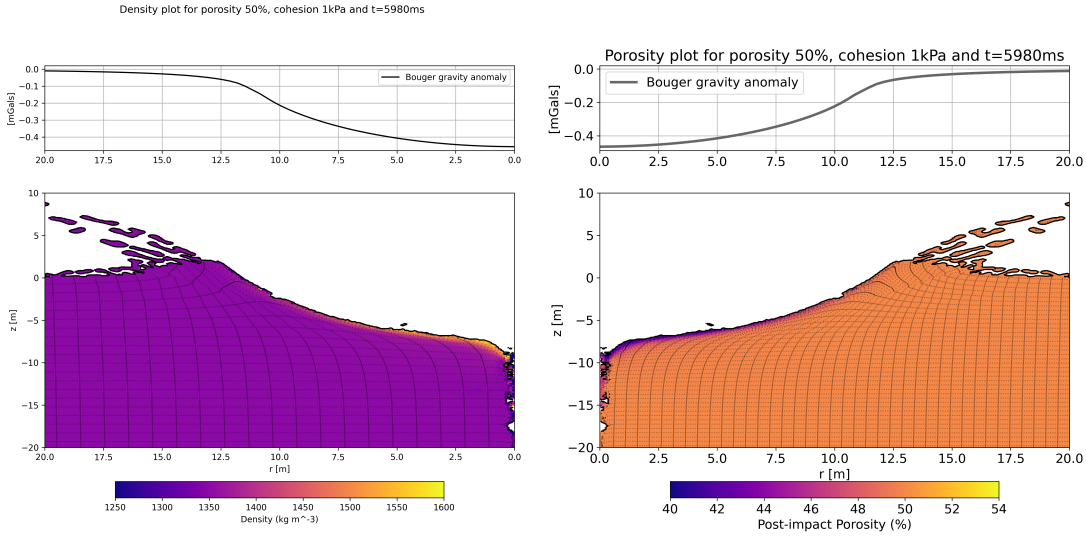

(a) Density (b) Porosity

Figure 14: Bouguer anomalies for 50% 1 kPa case

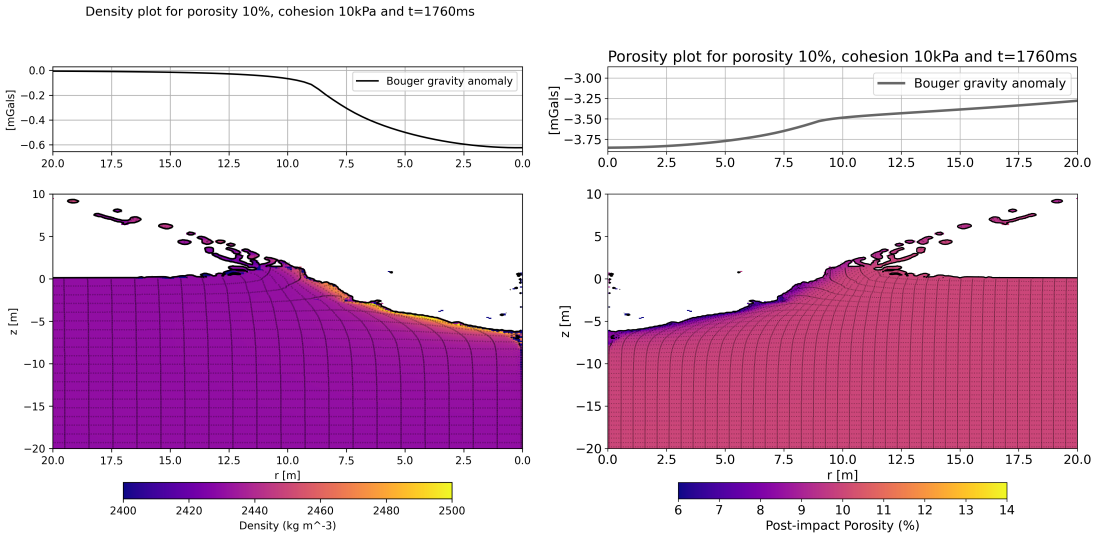

(a) Density (b) Porosity

Figure 15: Bouguer anomalies for 10% 10 kPa case

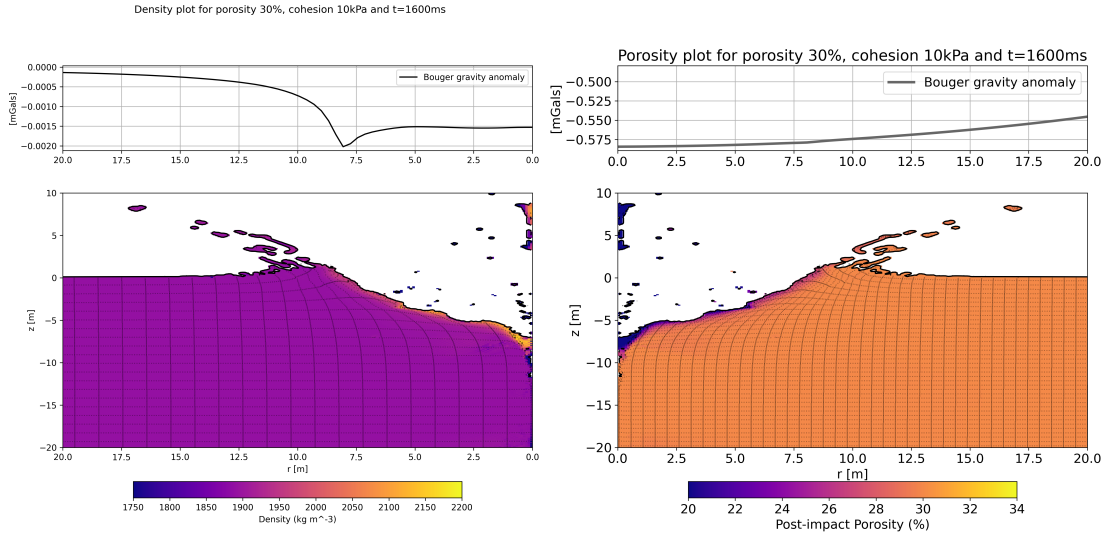

(a) Density (b) Porosity

Figure 16: Bouguer anomalies for 30% 10 kPa case

The unusual profile for the density seems to come from the central mound geometry of the crater. We can see a lot of material from the impact point still floating, having probably detached itself from the centre.

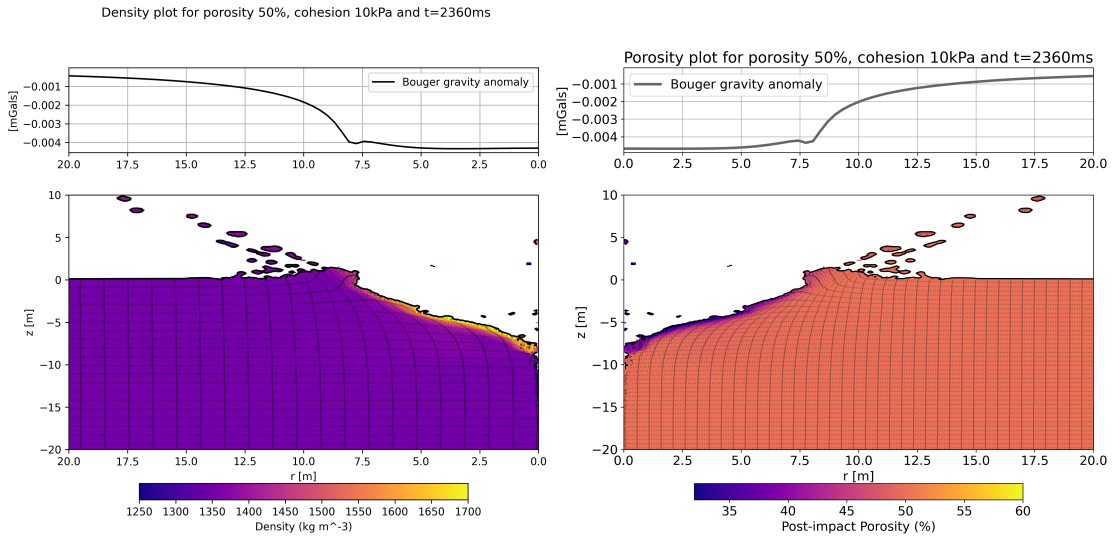

(a) Density (b) Porosity

Figure 17: Bouguer anomalies for 50% 10 kPa case

Fig. 17 has a peculiar Bouguer anomaly profile. This could be due to the geometry of the crater, which resembles either a concentric or a flat-bottom crater, as we can see the sharp drops at 7.5 m from the impact centre.

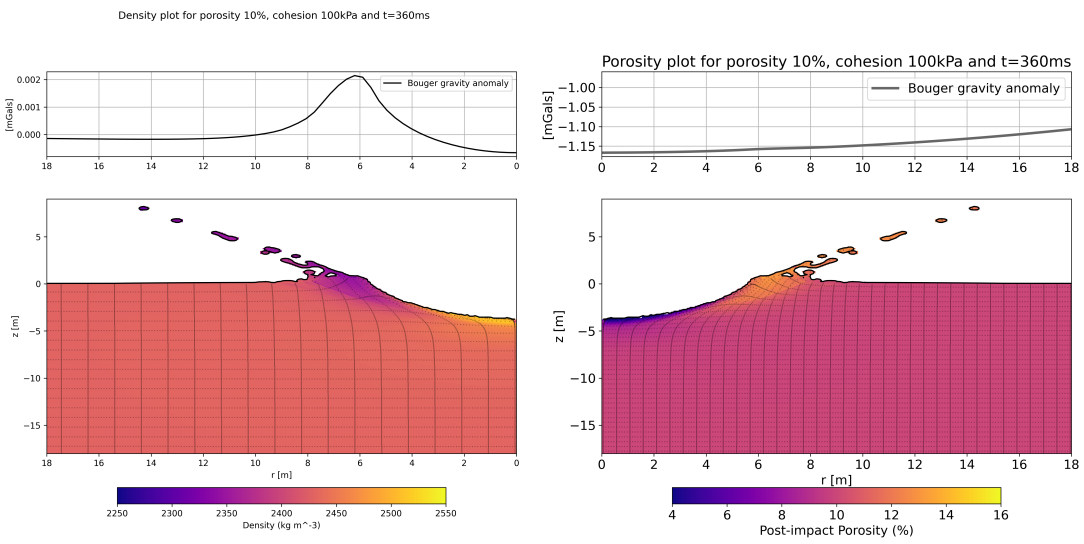

(a) Density (b) Porosity

Figure 18: Bouguer anomalies for 10% 100 kPa case

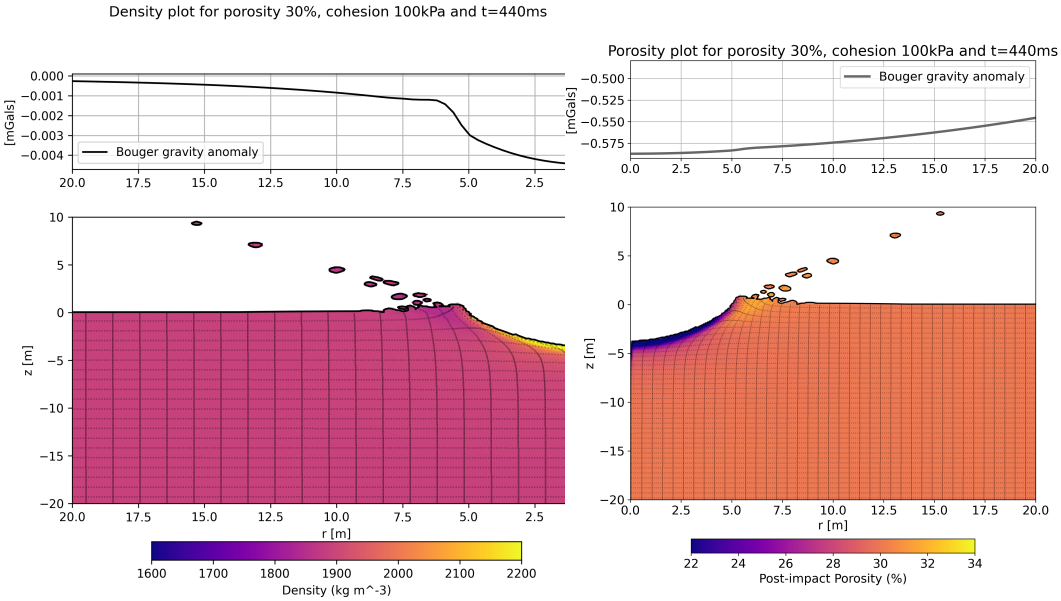

(a) Density (b) Porosity

Figure 19: Bouguer anomalies for 30% 100 kPa case

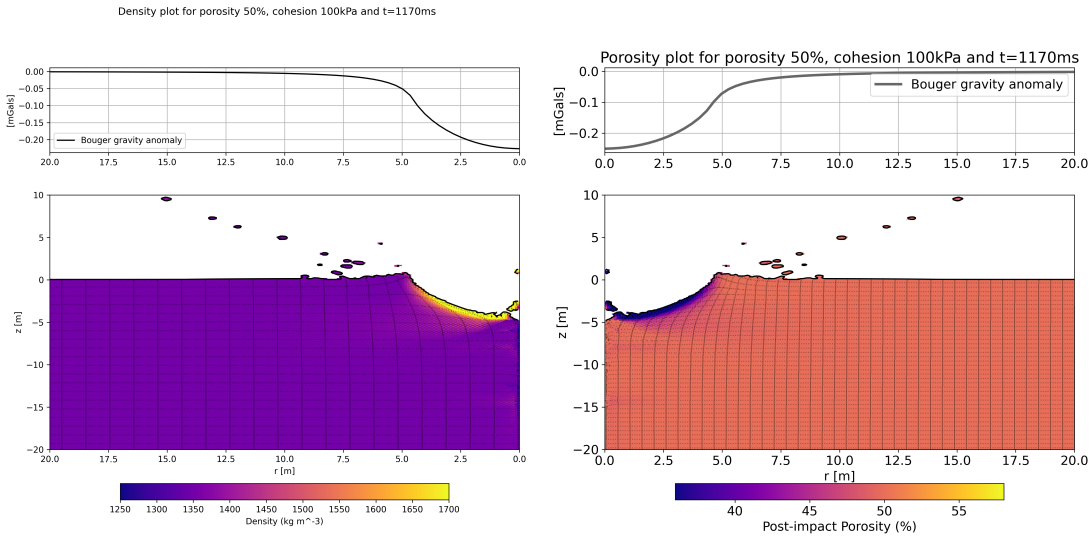

(a) Density (b) Porosity

Figure 20: Bouguer anomalies for 50% 100 kPa case

The anomalies in Figs 15, 16, 18 and 19 are very different from one calculation to the other. As mentioned, they all use the same reference density to calculate the mass between the measurement point and the reference ellipsoid, in the case of geophysics. But for Dimorphos, this reference should not be the same. PySALEPlot must have an appropriate approximation for small bodies such as Dimorphos. Since the parameters used to compute these anomalies are not clear, my assumption is that different approximations are done based on whether the input data is a density or a porosity. That is why even in the other cases where the curves follow the same trend, the magnitudes are different.

4.2 Gravity Shape Models

The last set of results is the shape models of Dimorphos containing the gravitational potential computations in J kg^{-1}. Recall that the cases shared by Luther et al. 2022 have the parameters as in Table 3. The SBMT pictures based on the paper's iSALE impact simulations are shown in Appendix A.4 with 50% and 10% porosity.
To get the gravitational potential from the PGM, I needed to input the shape model of Dimorphos containing the impact crater. This shape model, made in Blender by combining the oblate spheroid shape of Dimorphos with the impact crater by Mz Tasev, is hollow at the core. The gravitational potential is computed from that in units of Joules per kilogram. The portions of Dimorphos furthest away from the core have the least negative values. This is because potential approaches the asymptote at 0 the farther you go from the mass.

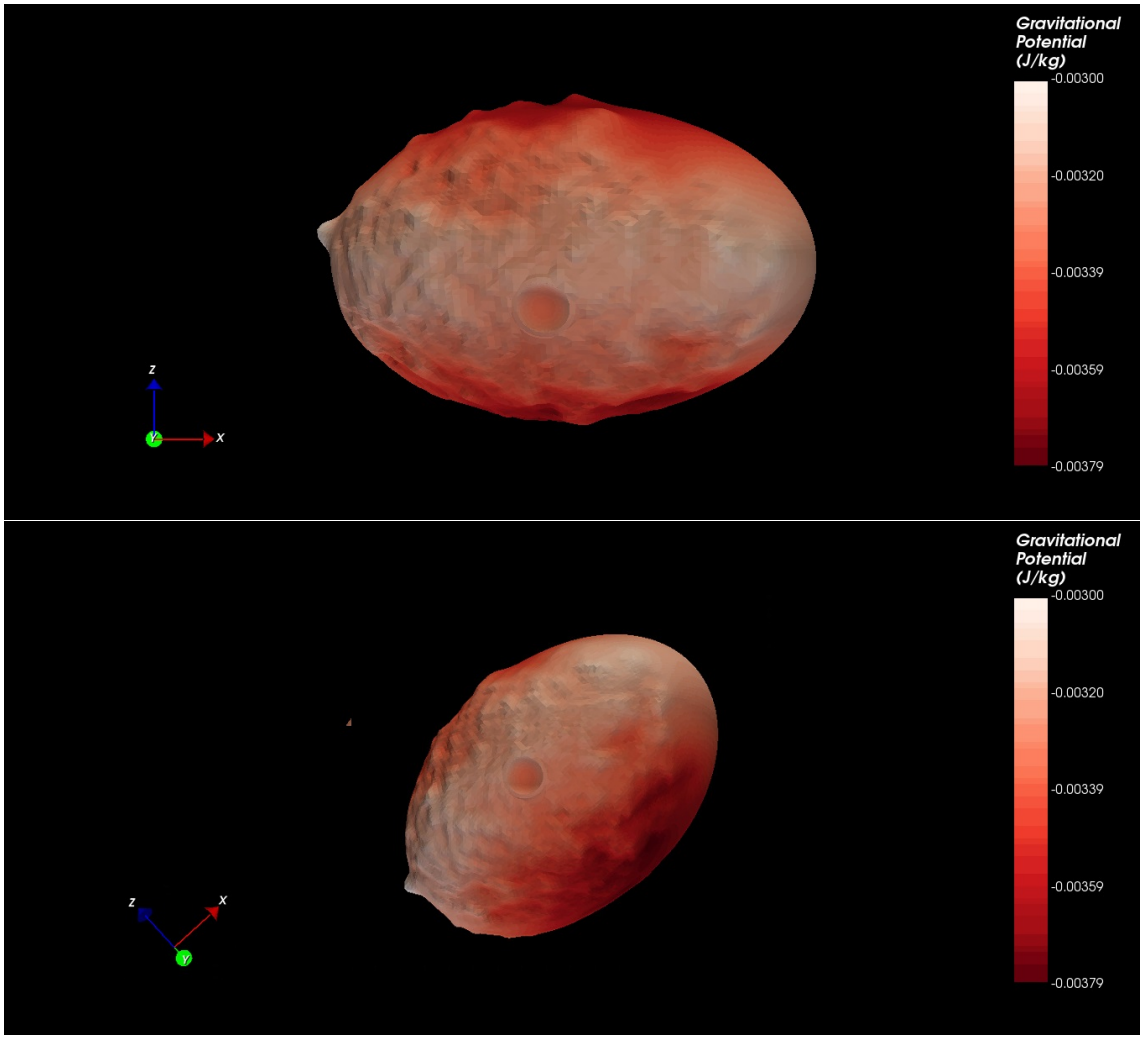

Figure 21: SBMT colour map of $Y = 100$ kPa, $\phi = 30\%$ case

We can see in Figs 21, 22, 23 that the radius of the impact crater increases as cohesion decreases, just like in the two-dimensional plots (e.g. the 30% cohesion cases in Figs 9b, 10b, 11b).

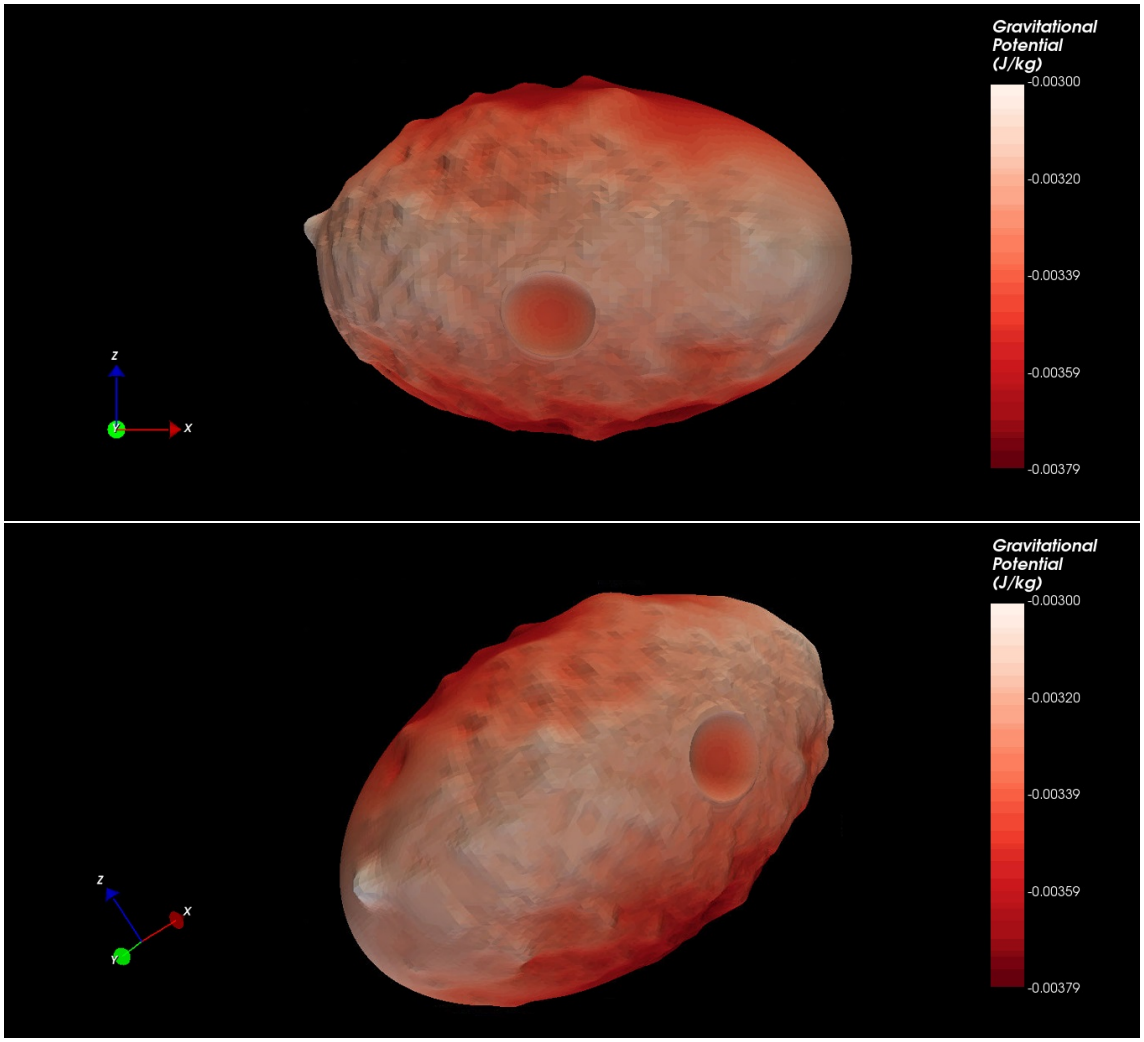

Figure 22: SBMT colour map of $Y = 10$ kPa, $\phi = 30\%$ case

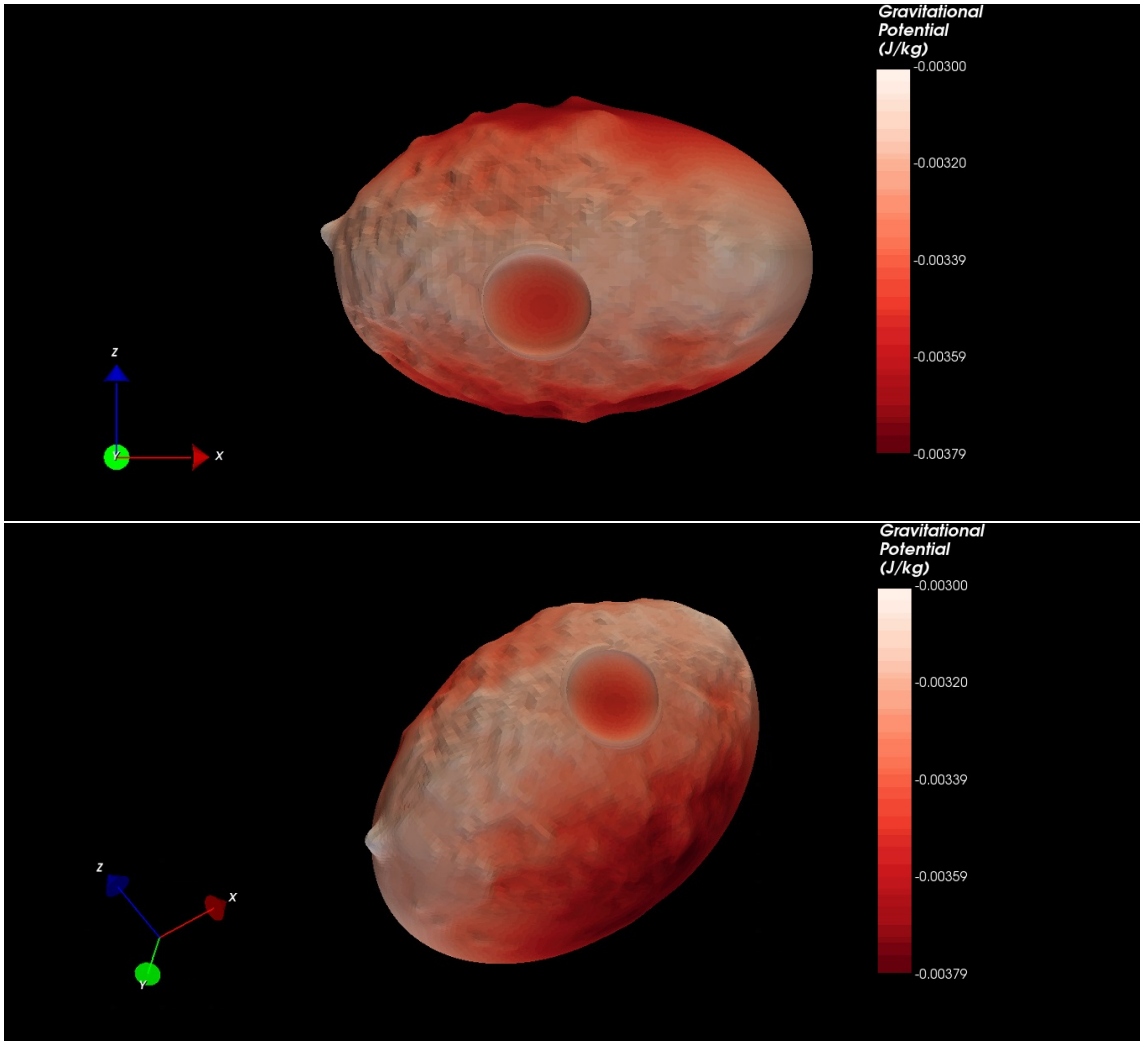

Figure 23: SBMT colour map of $Y = 1$ kPa, $\phi = 30\%$ case

The change in gravitational potential is quite small; the craters have a change on the order of $< 10^{-3}$ J kg^{-1}, perhaps 2×10^{-4} J kg^{-1}, although it is hard to tell. Most variations in the potential occur on the surface of Dimorphos, not in the crater. This suggests that these craters do not change the mass of the moonlet to a noticeable degree. We can see the high potential regions (more negative) along the "poles" when looking with the z-axis pointing up, as well as the low potential equatorial region (less negative). A potential closer to 0 means the surface is further away from the core of the body, or the centre, whereas one that is more negative shows it is nearer. This is visible in the craters as well: the raised edges are further away from the core and have a smaller magnitude of gravitational potential than the deep crater areas. Overall, the crater does not seem to impact the range of gravitational potential of the moonlet, but it should be noticeable as it is in the "equatorial" region that has an overall smaller magnitude in potential

than both the poles and the depths of the crater.

5 Conclusion

The results shown are quite consistent with other studies concerning how the crater dimensions change with increasing porosity and cohesion. We saw the change in crater diameters and crater depth but also two different geometries. Not all the simulations ran for the same amount of time and some were maybe halted a bit too early, so it is hard to form definitive conclusions as to what the crater shapes on Dimorphos are really like. The parameters used for the cohesion are also much larger than what we would expect for a rubble pile asteroid, which is what Dimorphos is assumed to be. The Bouguer anomalies unfortunately do not provide much insight as more work is required to correctly process the data from the density and porosity results.
The gravitational potential results require more work to give concrete numbers on detectable variations on Dimorphos due to the impact crater because the current colour maps do not show enough precision to determine to what degree a change would be noticeable. The SBMT maps are however a great way to visualise the crater on the moonlet in three dimensions and, with some imagination, give us a possible glimpse into what Hera will one day see as she arrives at her destination.
This thesis has successfully combined the crater morphology simulations in two dimensions with the gravity computations from shape models in three dimensions. Although the process is currently inefficient, time-consuming and computation heavy, it can be refined and automated to give us the possible gravity anomalies on Dimorphos due to DART.

5.1 Improvements & Future Work

Although this thesis work contains a lot of results, it is only the beginning. I would like to highlight some areas I think I could improve on as well as expand:

- The gravity anomaly results are not useful in this state as the results are not consistent depending on if they are computed from density data or porosity data. I would like to spend more time refining the pySALEPlot scripts and reaching out to the developers. In this way, we can make full use of all the data available from the two-dimensional simulations, such as other gravity anomalies.

- Combining the two-dimensional impact crater simulations with the three-dimensional gravity models by Ms Tasev was a proof of concept. Now that it has been demonstrated to be feasible, we hope that it can be developed further and maybe turned into a pipeline. Currently, the problem lies in the 3D modelling aspect. Ms Tasev had to model the impact crater by

hand in the program called Blender. Because of this, she cared mostly about getting the proper crater diameter and depth, as well as the edge or ridge that appears above ground. She did not necessarily try to replicate exact intricate morphologies inside the crater. If there is an automated way to do this, many more craters can be turned into shape models and have the exact geometry that was simulated.

- Thanks to Luther et al. 2022, Ms Tasev was able to model the 10% and 50% porosity cases. This was done because I had not yet finished running all my iSALE simulations at the time. Once I finished, she made the batch of 30% porosity. An obvious next step would be to compute the 6 other cases and then compare them to the Luther et al. results, as we used slightly different parameters in the simulations.

- Time was a huge factor influencing my work. I would have liked to get more familiar with the PGM to then plot different parameters in SBMT. At some point in time, I tried to set up a 2-layer iSALE scenario, like the Raducan et al. 2020 paper. However, I had to leave it and concentrate on the primary focus of my thesis. This would be nice to explore in the future. I did not use any SPH codes either, which would have been good to try, had I had more time.

- Our cohesion cases are relatively high compared to what we can expect from a rubble-pile asteroid. The obvious reason for that is computation time: more cohesive targets are easier to simulate in iSALE. However to get a good idea of what Hera could expect in 2026 as it arrives near the moonlet, low cohesion simulations need to be done. The iSALE simulations of 1 kPa took weeks each to complete, so it is not realistic to have low cohesions such as 100 or 10 Pa using this program. I believe SPH codes such as Bern SPH are better suited for these very low porosities.

- During the first ideation meeting between Dr Senel, Dr Karatekin and me, we thought we could have another phase in between the 1-layer iSALE simulations and the PGM phase. It would have consisted of simulating the same cases but not on a flat surface, but rather on a two-dimensional curved ellipsoid representing Dimorphos. The idea was to have the appropriate curvature. This would have helped Ms Tasev in her shape models as well: one challenge she encountered was trying to fit the impact craters which were made on a flat surface onto a curved Dimorphos model.

Afterword

My thesis experience is the culmination of my studies. From my Bachelor of Science with a major in Astronomy, to my Master's in Space Sciences focusing on

gaining professional experience through internships and working with an institute other than ULiège, my trajectory has taken 6 years.
Thanks to my supervisor Dr Senel, I was allowed to use the high-performance computing (hpc) machines at ROB remotely which allowed me to avoid commuting to Bruxelles to work on my thesis. It however also meant I had less contact with the researchers there and that administrative procedures took a lot more time. It also meant that my technical problems took longer to fix. However, working remotely allowed me to continue to attend my courses and work from wherever I wanted. I greatly appreciate all the time, effort and trust Dr Senel has dedicated to me and my thesis this year. All in all, I am really happy with what I managed to achieve and present in this report. I have learned a lot of what I set out to do and am looking forward to whatever comes next.

Acknowledgements

My greatest gratitude to my supervisors at ROB: Dr Cem Berk Senel for helping me set up the iSALE-Dellen environment and the scripts, giving me access to ROB facilities and resources and for guiding and leading me through the entirety of my thesis and Ms Elisa Tasev for sharing your polyhedron gravity model for me to use and taking the time to help me in the computations and interpretation of the results as well as teaching me how to use the SBMT. Thank you to Dr Özgür Karatekin for promoting this master thesis topic. My apologies to the staff at ROB for using all the hpc machines' memory for my simulations.
My appreciation to Dr Denis Grodent at ULiège for giving me guidance and advice in writing the thesis structure and filling the vacant supervisor position after the unfortunate accident of Dr Emmanuël Jehin.
Thank you to my parents and siblings for the motivation and support throughout my studies and for encouraging me to persist.
Much obliged to Ms Kristel Karemans and Dr Michaël De Becker for the administrative help and guidance.
As the iSALE-Dellen code is distributed on a case-by-case basis, we gratefully acknowledge the iSALE developer team for their contribution (Amsden et al., 1980 [1]; Wünnemann et al., 2006 [33]; Collins et al., 2004 [6]; Ivanov et al., 1997 [20]; Melosh et al., 1992 [23]).
A sincere thank you to Dr Robert Luther, Dr Sabina Ruducan and the co-authors for sharing their figures.

Abbreviations

AIDA Asteroid Impact & Deflection Assessment

AIM Asteroid Impact Mission

ASI Agenzia Spaziale Italiana

DART Double Asteroid Redirection Test

EoS equation of state

ESA European Space Agency

GRASS Gravimeter for Small Solar system bodies

hpc high-performance computing

JAXA Japanese Aerospace Exploration Agency

KBO Kuiper-belt object

LICIACube Light Italian Cubesat for Imaging of Asteroids

MBA Main-belt asteroid

MMX Martian Moons eXploration

NASA National Aeronautics and Space Administration

NEO near-Earth object

PGM Polyhedron gravity model

ROB Royal Observatory of Belgium

SBMT Small Body Mapping Tool

SPH smooth particle hydrodynamics

ULiège the University of Liège

YORP Yarkovsky–O'Keefe– Radzievskii–Paddack

References

[1] Amsden, A.; Ruppel, H.; Hirt, C. "SALE: A simplified ALE computer program for fluid flow at all speeds." *Los Alamos National Laboratories Report*, LA-8095, pp 101 (1980) Los Alamos, New Mexico: LANL.

[2] Cheng, A.F.; Michel, P.; Jutzi, M.; Rivkin, A.S.; Stickle, A.; Barnouin, O.; Ernst, C.; Atchison, J.' Pravec, P.; Richardson, D.C.; AIDA team; AIM team. "Asteroid Impact & Deflection Assessment mission: Kinetic impactor." *Planetary and Space Science* 121, pp 27-35 (February 2016). Elsevier https://doi.org/10.1016/j.pss.2015.12.004

[3] Cheng, Andrew F.; Raducan, Sabina D.; Fahnestock, Eugene G.; Dotto, Elisabetta; Della Corte, Vincenzo; Stickle, Angela M. "Model of Double Asteroid Redirection Test Impact Ejecta Plume Observations." *The Planetary Science Journal*, 3, 6 (June 2022). American Astronomical Society. https://iopscience.iop.org/article/10.3847/PSJ/ac66e9

[4] Cheng, A.F.; Agrusa, H.F.; Barbee, B.W.; et al. "Momentum transfer from the DART mission kinetic impact on asteroid Dimorphos." Nature, vol 616, pp457 – 460 (20 April 2023). https://doi.org/10.1038/s41586-023-05878-z

[5] Collins, G.S.; Elbeshausen, D.; Wünnemann, K.; Davison, T.M.; Ivanov, B.; Melosh, H.J. "iSALE: A multi-material, multi-rheology shock physics code for simulating impact phenomena in two and three dimensions." (8 July 2016) iSALE-Dellen Manual. DOI:10.6084/m9.figshare.3473690.v2 .

[6] Collins, G. S.; Melosh, H. J.; Ivanov, B. A. "Modeling damage and deformation in impact simulations." *Meteoritics and Planetary Science*, 39, pp 217–231 (2004).

[7] Collins, G.; Melosh, H. J.;Wünnemann, K. "Improvements to the epsilon-alpha compaction model for simulating impacts into high-porosity solar system objects". *International Journal of Impact Engineering*, 38, 6, pp 434–439 (2011).

[8] [Collins, G. S. "Numerical simulations of impact crater formation with dilatancy." *Journal of Geophysical Research – Planets*, 119, pp 2600–2619 (2014).

[9] De Pater, I.; Lissauer, J.J. "Minor Planets." *Planetary Sciences*, 2nd edition, Cambridge University Press, pp. 366-402 (January 2015), Cambridge, United Kingdom. ISBN: 978-1-107-09161-0 https://doi.org/10.1017/CBO9781316165270.010

[10] Elbeshausen, D.; Wünnemann, K.; Collins, G. S. "Scaling of oblique impacts in frictional targets: Implications for crater size and formation mechanisms." *Icarus*, 204,2, pp 716–731 (2009).

[11] Ernst, C.M. et alia. "The Small Body Mapping Tool (SBMT) for Accessing, Visualizing, and Analyzing Spacecraft Data in Three Dimensions." *LPSC*, 49, abstract 1043 (2018).

[12] "GRASS gravimeter (HERA)." *ROB Opendoors* (2022). https://www.astro.oma.be/opendoors/posters/planetology/Poster_HERA_GRASS_2022.pdf Poster, French and Dutch.

[13] Hackney, Ron. "Gravity, Data to Anomalies." *Encyclopedia of Solid Earth Geophysics*, pp 524–533 (2011), edited by Harsh K. Gupta, Encyclopedia of Earth Sciences Series. Springer, Dordrecht, Netherlands. Online since 1 Jan 2014 https://doi.org/10.1007/978-90-481-8702-7_78

[14] "Hera." *Space Safety*, ESA (2022) https://www.esa.int/Space_Safety/Hera/Hera

[15] Housen, Kevin R.; Holsapple, Keith A. "Ejecta from impact craters." *Icarus* vol 211,1, pp856-875 (January 2011). Elsevier https://doi.org/10.1016/j.icarus.2010.09.017

[16] Madeira, Gustavo; Charnoz, Sébastien; Hyodo, Ryuki. "Dynamical origin of Dimorphos from fast spinning Didymos." Icarus vol 394 (April 2023). Elsevier https://doi.org/10.1016/j.icarus.2023.115428

[17] Naidu, S.P. ; Benner, L.A.M., Brozovic, M.; et al. "Radar observations and a physical model of binary near-Earth asteroid 65803 Didymos, target of the DART mission." Icarus, vol 348 (15 September 2020). https://doi.org/10.1016/j.icarus.2020.113777

[18] "In Depth | Didymos." *NASA Solar System Exploration*, NASA (14 Oct 2022). https://solarsystem.nasa.gov/asteroids-comets-and-meteors/asteroids/didymos/in-depth/

[19] "Instrument to measure asteroid gravity tested for space." *Space Safety / Hera*, ESA (22 May 2023). https://www.esa.int/Space_Safety/Hera/Instrument_to_measure_asteroid_gravity_tested_for_space .

[20] Ivanov, B. A.; Deniem, D.; Neukum, G. "Implementation of dynamic strength models into 2D hydrocodes: Applications for atmospheric breakup and impact cratering." *International Journal of Impact Engineering*, 20, pp 411–430 (1997).

[21] Lompa, T.; Wünnemann, K.; Wahl, D.; Padovan, S.; Miljković, K. "Numerical Investigation of Lunar Basin Formation Constrained by Gravity Signature." *Journal of Geophysical Research: Planets* 126, 11 (20 Oct 2021). DOI: e2021JE006908 https://doi.org/10.1029/2021JE006908

[22] Luther, R.; Raducan, S.D.; et alia. "Momentum Enhancement during Kinetic Impacts in the Low-intermediate-strength Regime: Benchmarking and Validation of Impact Shock Physics Codes." *The Planetary Science Journal*, 3,

227 (October 2022). American Astronomical Society.
https://doi.org/10.3847/PSJ/ac8b89

[23] Melosh, H. J.; Ryan, E. V.; Asphaug, E. "Dynamic fragmentation in impacts: Hydrocode simulation of laboratory impacts." *Journal of Geophyical Research*, 97(E9), pp 14735–14759 (1992).

[24] Quaide, William L. & Oberbeck, Verne R. "Thickness Determinations of the Lunar Surface Layer from Lunar Impact Craters."
Journal of Geophysical Research, vol 73, 16, pp 5247 - 5270 (15 August 1968). American Geophysical Union. DOI: 10.1029/JB073i016p05247
https://doi.org/10.1029/JB073i016p05247

[25] Raducan, S.D.; Davison, T.M; Collins, G.S. "The effects of asteroid layering on ejecta mass-velocity distribution and implications for impact momentum transfer." *Planetary and Space Science* 180, 104756 (January 2020). Elsevier
https://doi.org/10.1016/j.pss.2019.104756

[26] Raducan, S.D.; Jutzi, M.; Davison, M.; et alia. "Influence of the projectile geometry on the momentum transfer from a kinetic impactor and implications for the DART mission." *International Journal of Impact Engineering*, 374, 114793 (5 Jan 2022). arXiv:2201.01730v1

[27] Richardson, D.C.; Agrusa, H.F.; Barbee, B; et al. "Predictions for the Dynamical States of the Didymos System before and after the Planned DART Impact." *PSJ*, 3,7 pp 157(14 July 2022). American Astronomical Society DOI: 10.3847/PSJ/ac76c9
https://iopscience.iop.org/article/10.3847/PSJ/ac76c9

[28] Scheirich, P; Pravec, P. "Modeling of lightcurves of binary asteroids." *Icarus* vol 200, 2, 531-547 (April 2009). Elsevier https://www.sciencedirect.com/science/article/abs/pii/S0019103508004193

[29] Senel, C.B. et alia. "Post-Impact Porosity And Gravity Anomalies Following The Hypervelocity Dart Impact On Asteroid Dimorphos." *LPSC 2023*, Houston, USA (March 2023). Poster.

[30] Senel, C.B.; Karatekin, O.; Raducan, S.D.; Luther, R. "Post-Impact Porosity and Gravity Anomalies Following the Hypervelocity Dart Impact on Asteroid Dimorphos." *Royal Observatory of Belgium* (2023). Unpublished.

[31] Stickle, Angela M. ; DeCoster, Mallory E. ; et alia. "Effects of Impact and Target Parameters on the Results of a Kinetic Impactor: Predictions for the Double Asteroid Redirection Test (DART) Mission." *The Planetary Science Journal*, 3, 248 (November 2022). American Astronomical Society
https://doi.org/10.3847/PSJ/ac91cc

[32] Tasev, Elisa "Determination of the interior structure of small bodies of the Solar system." *Université Libre de Bruxelles* (2019). Master thesis.

[33] Wünnemann, K.; Collins, G.; Melosh, H. "A strain-based porosity model for use in hydrocode simulations of impacts and implications for transient crater growth in porous targets." *Icarus*, 180, pp 514–527 (2006).

A Appendix

A.1 Thesis Topic Proposal

Hypervelocity impact modeling of the solar system bodies.
Contact person: Promotor: Ozgur Karatekin, co-promotor: Cem Berk Senel, reader: V. Dehant
ozgur.karatekin@oma.be, cem.berk@oma.be, v.dehant@oma.be
Observatoire royal de Belgique et UCLouvain Tel: 02 373 0266 (V. Dehant)
Office: Royal Observatory of Belgium
Availability: Any time by teleconf; please email to decide when.
Thematic: Planetology
Description: The impact processes are ubiquitous in the solar system, as one of the primary mechanisms driving the evolution of asteroids and comets. From small meteorite impacts to gigantic Moon-forming collisions, the impact cratering formation holds key insights pointing out the dynamical history of our solar system from 4.6 billion years ago. Meanwhile, thanks to the rapid advance in numerical modeling as well as computational resources, high-resolution numerical models offer a powerful framework assisted by either ground-based or spacecraft observational studies.
Within this context, this master thesis deals with the numerical modeling of impact processes by making use of state-of-the-art iSALE shock physics code as well as an N-body smoothed particle hydrodynamics (SPH) model. Performed simulations aim to resolve the aftermath of impacts on a variety of solar system bodies from asteroids to main belt comets and planetary moons, such as Phobos and Europa. This study offers a unique opportunity to better understand the solar system impact processes, ranging from cratering morphology towards the ejecta dynamics, volatile exchange, momentum transfer and interior dynamics. This work may lead to a scientific publication and can be extended through a doctoral thesis.
Task description:

- Perform shock physics model and N-body SPH model simulations.
- Implementing ANEOS/Tillotson equation of state (EOS) models.
- Comparison with the analytical, laboratory or in-situ scaling relations.
- Post-processing of simulation results by in-house and new algorithms in Python.

Master thesis subject proposal for the academic year of 2022-2023 by ROB.

A.2 Initial iSALE2D Plots

The results of the initial simulations I did appear here. These correspond to only 100 milliseconds of integration time in the *iSALE2D* simulations. The greatest

takeaway from this set is that the crater shapes had not yet reached their final form. However, doing more integration time required more computing power and reserved time on the hpc machines.

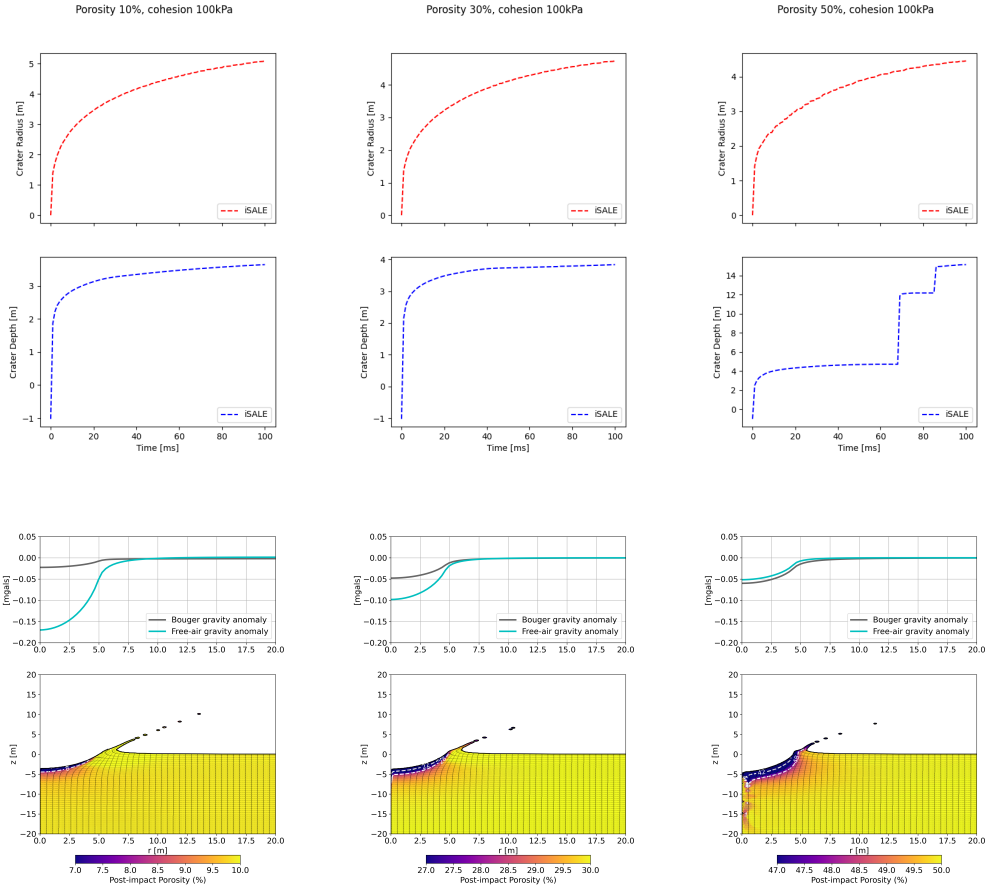

(a) $Y_{d0} = 100$ kPa, $\phi = 10\%$ (b) $Y_{d0} = 100$ kPa, $\phi = 30\%$ (c) $Y_{d0} = 100$ kPa, $\phi = 50\%$

Figure 24: 100 kPa cases before crater settled

Figure 24a shows the crater dimension evolution for a porosity percentage of 10% and a cohesion of 100 kPa for Dimorphos.
Figure 24b contains the initial results for a porosity of 30% and a cohesion of 100 kPa.
We have a porosity of 50% and a cohesion of 100 kPa in Fig. 24c.
The 6 other initial runs account for the cases 1 & 10 kPa of cohesion and 10, 30 & 50 % porosity, in the figures 26a,26b,26c and 25a,25b,25c respectively.

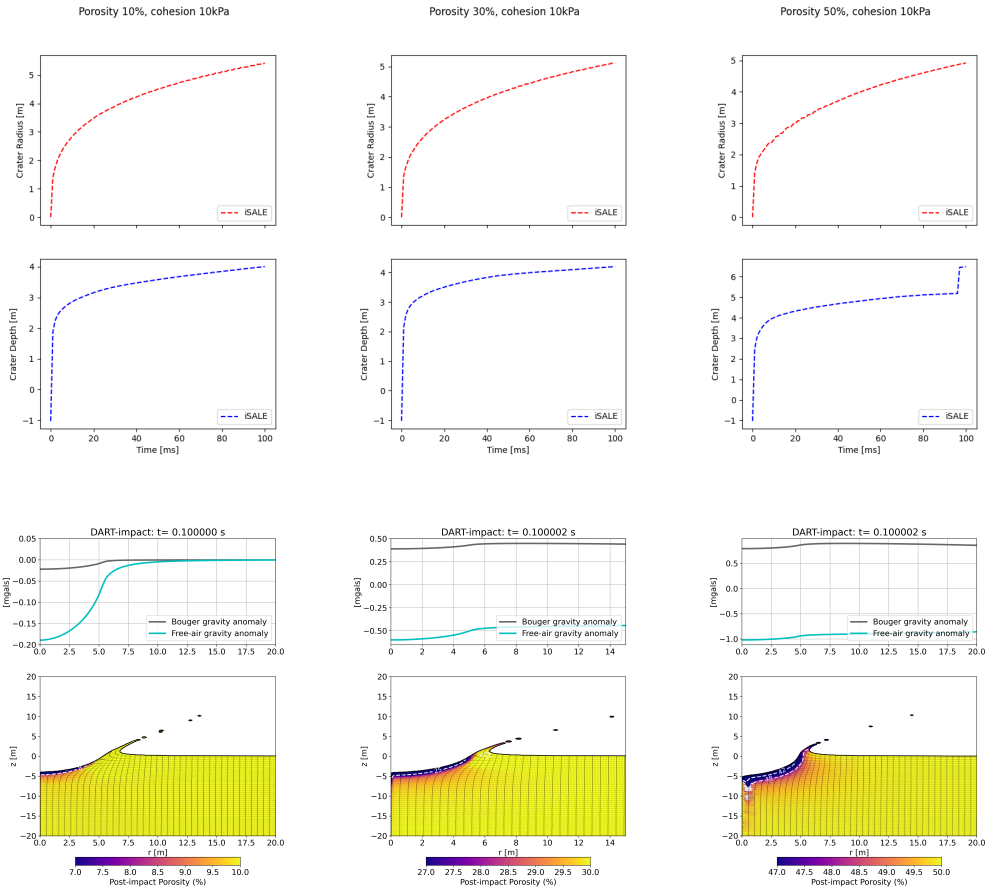

(a) $Y_{d0} = 10$ kPa, $\phi = 10\%$ (b) $Y_{d0} = 10$ kPa, $\phi = 30\%$ (c) $Y_{d0} = 10$ kPa, $\phi = 50\%$

Figure 25: 10 kPa cases before crater settled

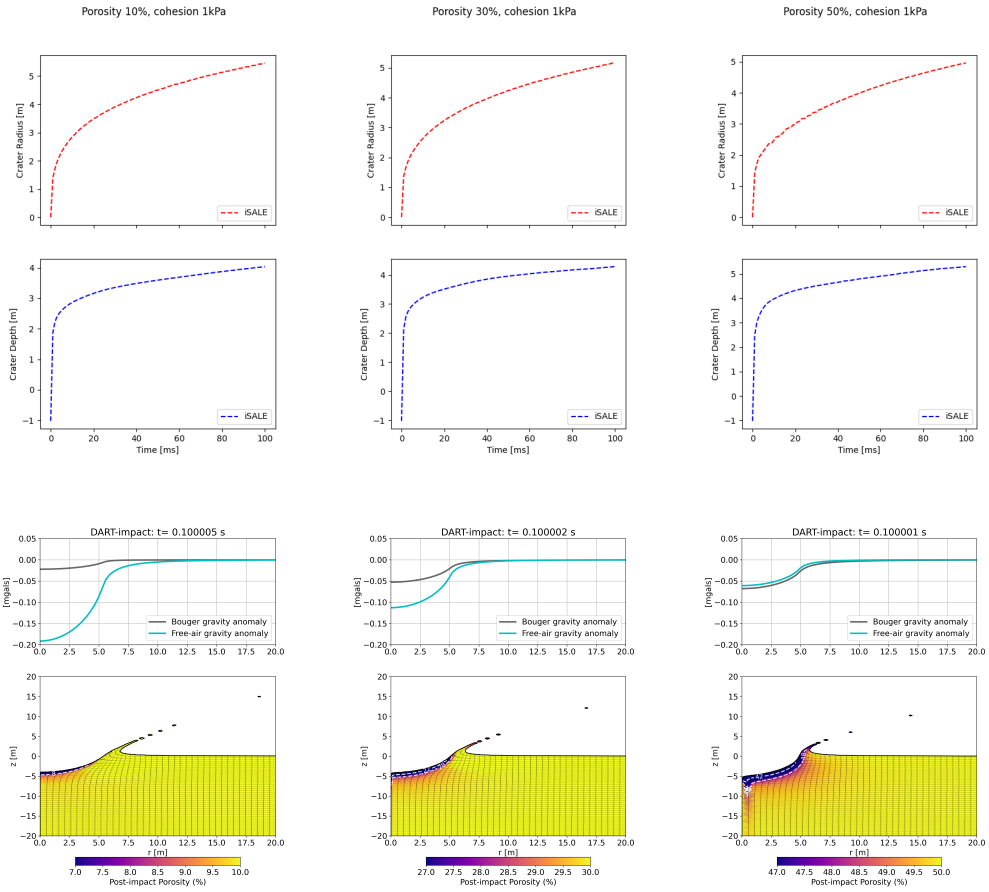

(a) $Y_{d0} = 1$ kPa, $\phi = 10\%$ (b) $Y_{d0} = 1$ kPa, $\phi = 30\%$ (c) $Y_{d0} = 1$ kPa, $\phi = 50\%$

Figure 26: 1 kPa cases before crater settled

As can be seen, the crater evolution (characterised by changes in crater depth and diameter in the left-hand side figures) is still on an increasing trend at the end of our integration time of 100 ms. This signifies that were the simulations to continue further than the integration time of 100 ms, the crater's morphology should have changed, i.e. the crater has not settled into its final shape yet.
Determining the final crater shape is vital for the estimation of the local post-impact surface gravity of Dimorphos.
Nota Bene
The anomaly plots are wrong as they do not take the density of the grid space of the simulated Dimorphos into account.

A.3 More iSALE Plots

Density plot evolution of the $\phi = 50\%$, $Y = 100$ kPa case. The

following plots show the evolution of the density over a period of 1130 ms starting at impact (0 ms).

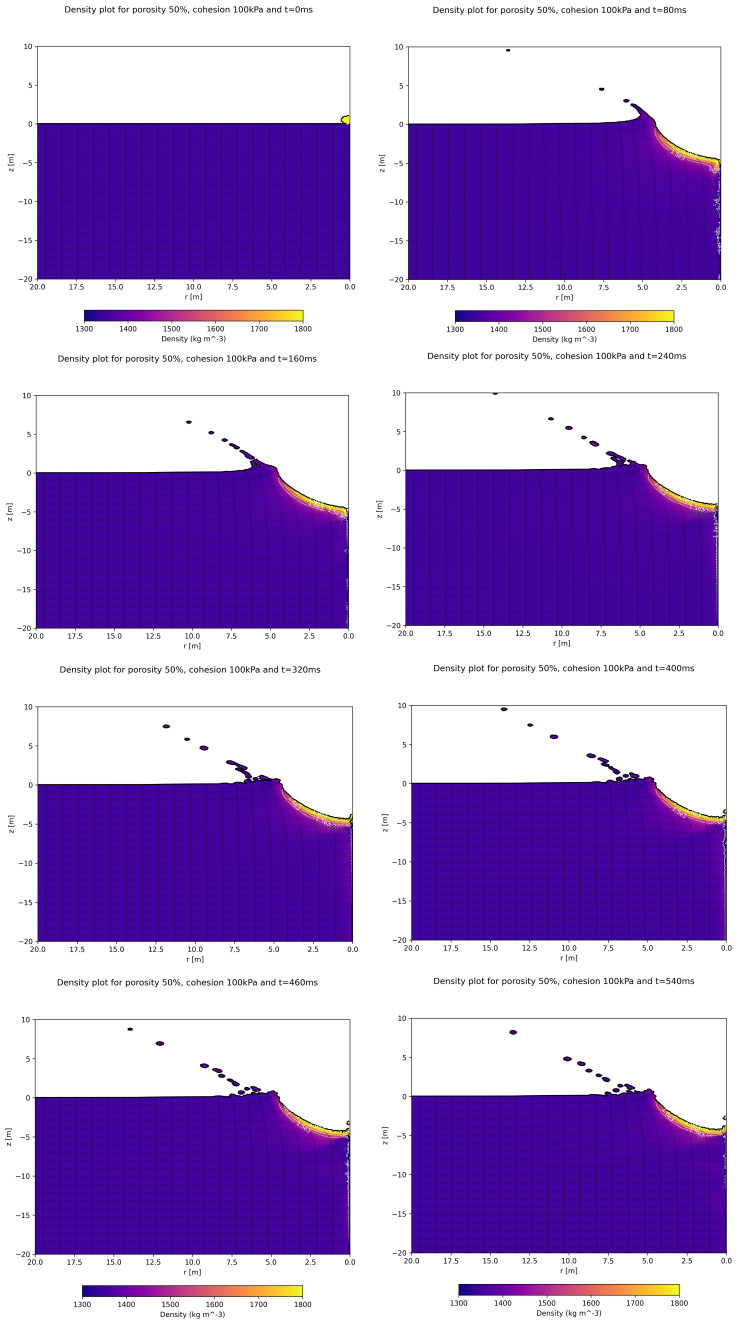

Figure 27: Plots of 50% 100 kPa crater morphology evolution through time

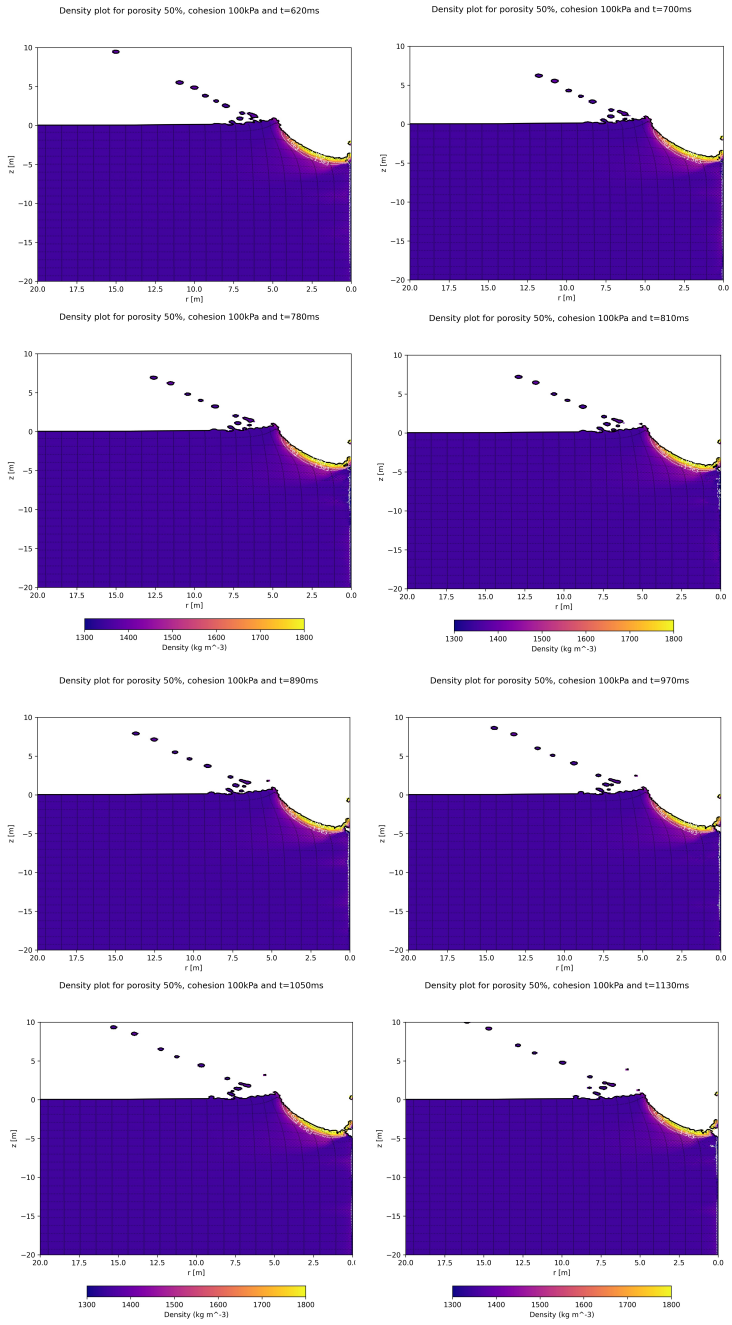

Figure 28: Plots of 50% 100 kPa crater morphology evolution through time

A.4 Gravity Shape Model Images

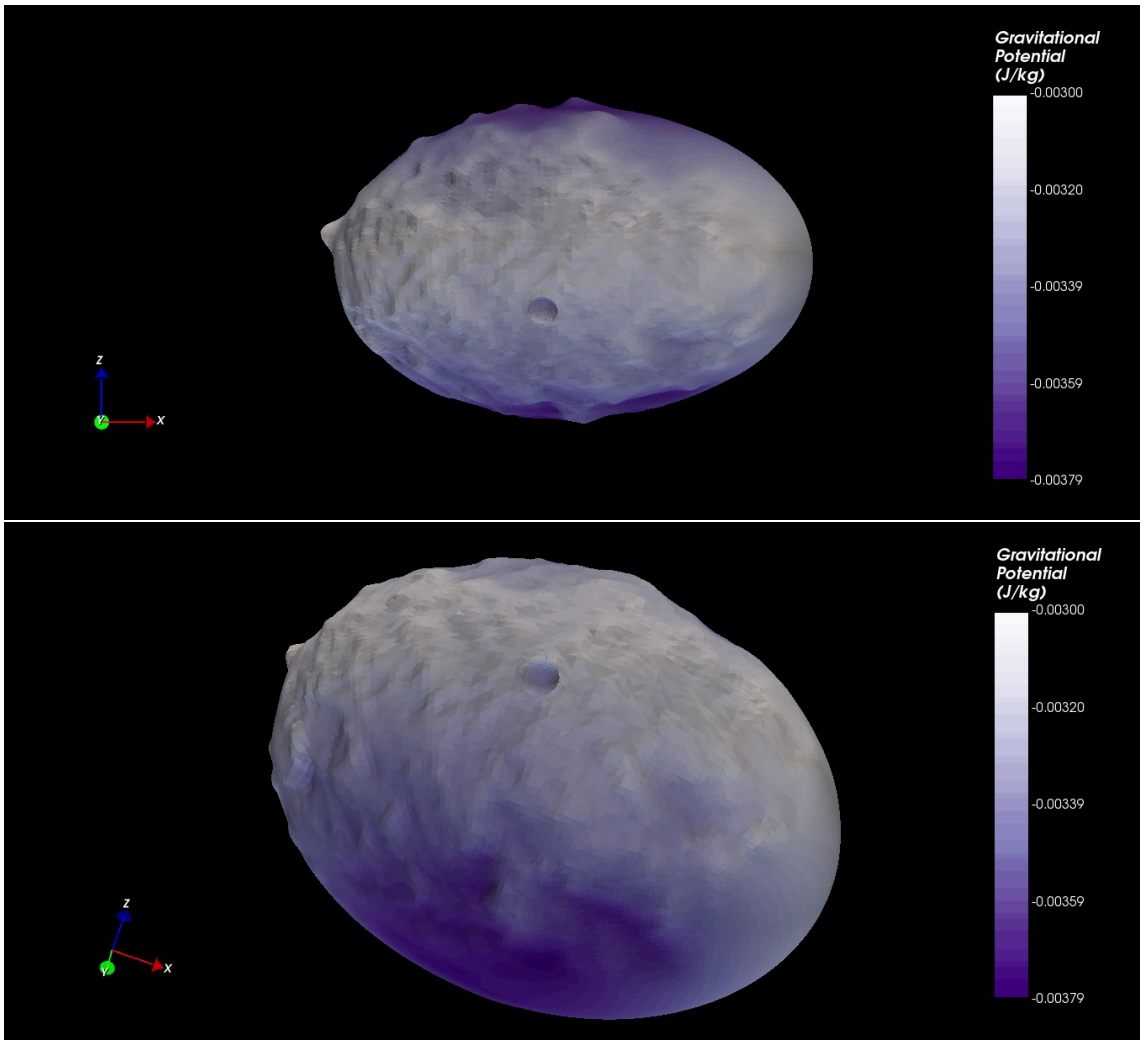

Figure 29: SBMT map of $Y = 100$ kPa, $\phi = 50\%$, modelled from Luther et alia 2022 [22]

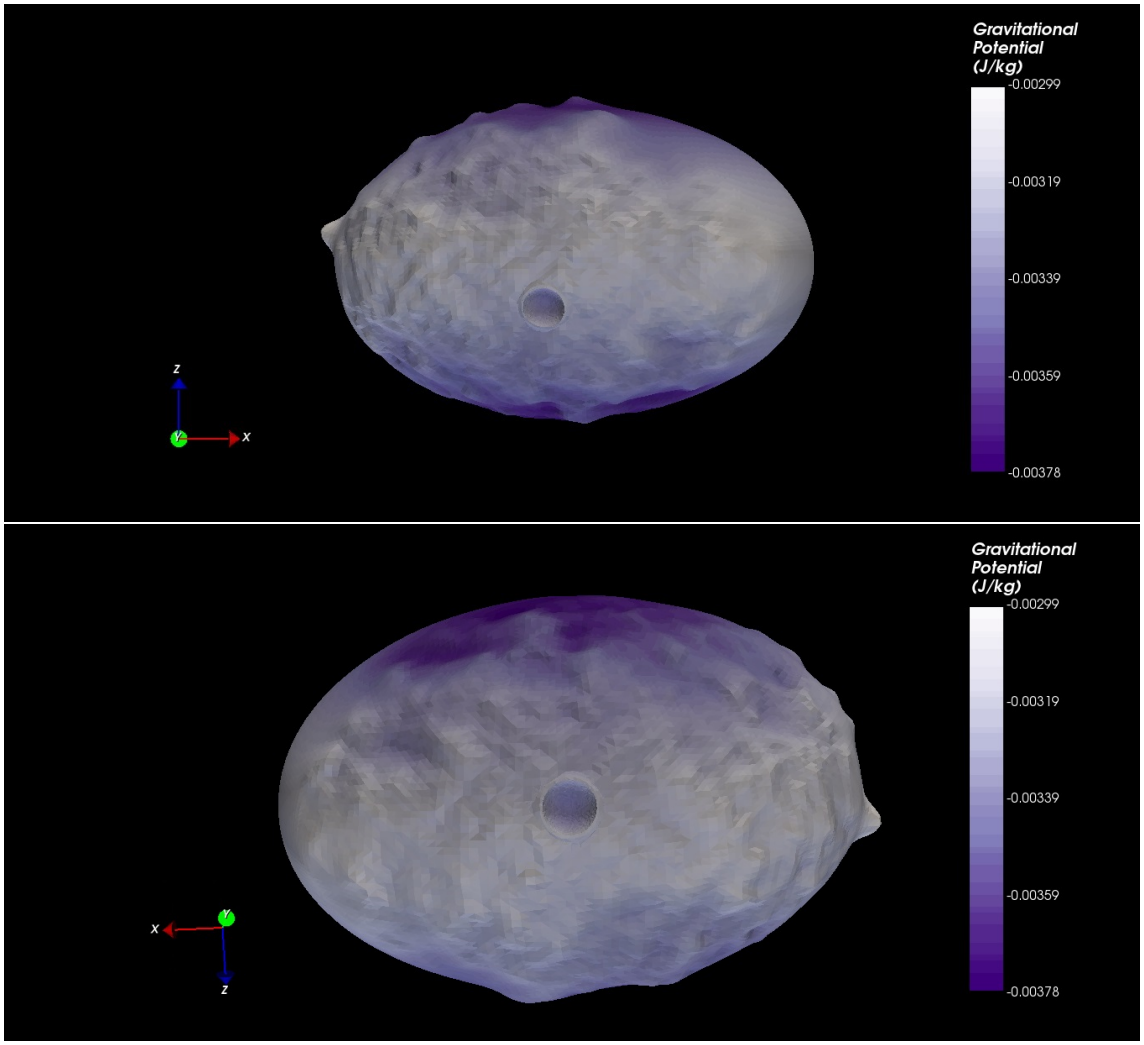

Figure 30: SBMT map of $Y = 10$ kPa, $\phi = 50\%$, modelled from Luther et alia 2022 [22]

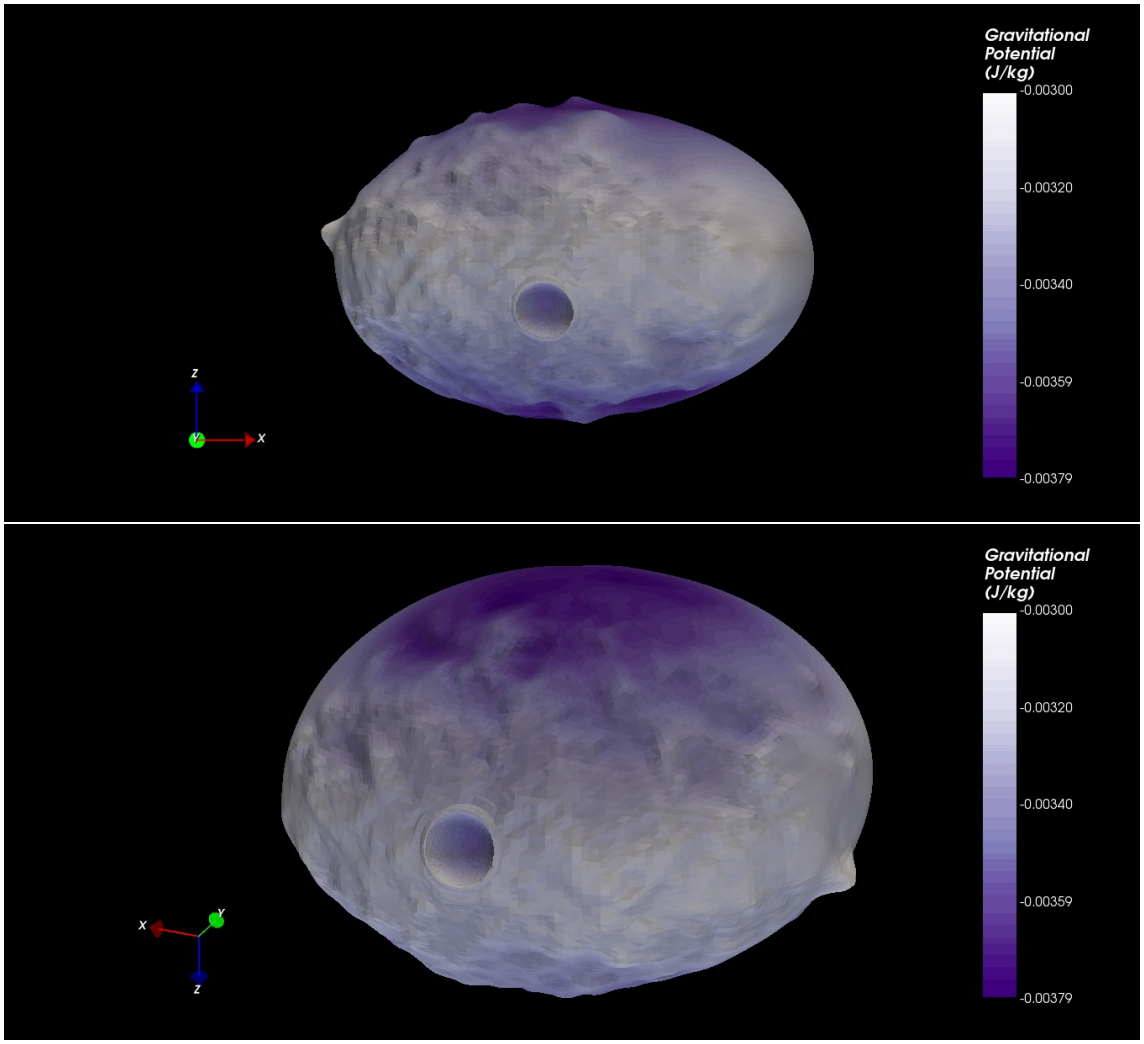

Figure 31: SBMT map of $Y = 1$ kPa, $\phi = 50\%$, modelled from Luther et alia 2022 [22]

A.5 Example iSALE Input Files

Model file 50% **100 kPa**

```
#ISINP
------------------------------------------------------------------------
--- this is the new input file used by iSALE versions of v7.0 and higher
------------------- General Model Info ---------------------------------
VERSION                __DO NOT MODIFY__              : 4.1
DIMENSION              dimension of input file        : 2
PATH                   Data file path                 : ./
MODEL                  Modelname                      : cg_dart03
```

```
TDUMP                    Dump save interval                : 5.0D-2
DUMP                     Restart with dump                 : cg_dart02/00081.dum
REGRID                   Regridding                        : 0
------------------ Mesh Geometry Parameters ------------------------
GRIDH                    horizontal cells                  : 0
: 300           : 40
GRIDV                    vertical cells                    : 40
: 600           : 0
GRIDSPC                  grid spacing                      : 1.023D-1
GRIDEXT                  ext. factor                       : 1.05d0
CYL                      Cylind. geometry                  : 1.0D0
------------------ Global setup parameters -------------------------
S_TYPE                   setup type                        : DEFAULT
T_SURF                   Surface temp                      : 288.0D0
DTDZSURF                 Surface temp. gradient (K/m)      : 10.D-3
D_LITH                   Thickness of lithosphere (m)      : 100.0D0
R_PLANET                 Radius of planet (m)              : 80.0D0
GRAD_TYPE                Lithostatic gradient              : DEFAULT
LP_TOLER                 Pressure tolerance                : 1.D-3
GRAV_V                   Gravitational acceleration        : -5.D-5
------------------ Projectile ("Object") Parameters ----------------
OBJNUM                   number of objects                 : 1
OBJRESH                  CPPR horizontal                   : 5
OBJRESV                  CPPR vertical                     : 5
OBJVEL                   object velocity                   : -6.5D3
OBJMAT                   object material                   : impactr
OBJTYPE                  object type                       : SPHEROID
------------------ Target Parameters -------------------------------
LAYNUM                   layers number                     : 1
LAYPOS                   layer position                    : 350
LAYMAT                   layer material                    : target_
LAYTPROF                 thermal profile                   : COND
EJECT_V                  ejecta elevation                  : 1.023
------------------ Time Parameters ---------------------------------
DT                       initial time increment            : 2.0D-3
DTMAX                    maximum timestep                  : 1.0D-1
TEND                     end time                          : 1.2D0
DTSAVE                   save interval                     : 4.0D-2
------------------ Boundary Condition Parameters -------------------
BND_L                    left                              : FREESLIP
BND_R                    right                             : FREESLIP
BND_B                    bottom                            : NOSLIP
```

```
BND_T                    top                                : OUTFLOW
------------------ Numerical Stability Parameters ----------------------
AVIS                     art. visc. linear                  : 0.20D0
AVIS2                    art. visc. quad.                   : 1.00D0
------------------ Tracer Particle Parameters --------------------------
TR_QUAL                  quality                            : 1
TR_SPCH                  tracer spacing X                   : 5.D0
TR_SPCV                  tracer spacing Y                   : 5.D0
TR_VAR                   add. tracer fiels                  : #TrP-TrT-TrA-TrV-Tr
------------------ (Material) Model parameters (global) ----------------
STRESS                   Consider stress                    : 1
PARTPRES                 Pres. in part.                     : 0
ADVECT                   Advect by mass or volume           : 1
VEL_CUT                  Velocity cutoff                    : -4.D0
------------------ Data Saving Parameters ------------------------------
QUALITY                  Compression rate                   : -50
VARLIST                  List of variables                  : #Den-Tmp-Pre-Sie-Yl
------------------------------------------------------------------------
<<END
```

Model file 30% **10 kPa**

```
#ISINP
------------------------------------------------------------------------
--- this is the new input file used by iSALE versions of v7.0 and higher
------------------ General Model Info ----------------------------------
VERSION                  __DO NOT MODIFY__                  : 4.1
DIMENSION                dimension of input file            : 2
PATH                     Data file path                     : ./
MODEL                    Modelname                          : gdart01_r1
TDUMP                    Dump save interval                 : 4.0D-2
DUMP                     Restart with dump                  : gdart01/00156.dump
REGRID                   Regridding                         : 0
------------------ Mesh Geometry Parameters ----------------------------
GRIDH                    horizontal cells                   : 0
: 300           : 40
GRIDV                    vertical cells                     : 40
: 600           : 0
GRIDSPC                  grid spacing                       : 1.023D-1
GRIDEXT                  ext. factor                        : 1.05d0
CYL                      Cylind. geometry                   : 1.0D0
------------------ Global setup parameters -----------------------------
S_TYPE                   setup type                         : DEFAULT
```

```
T_SURF              Surface temp                    : 288.0D0
DTDZSURF            Surface temp. gradient (K/m)    : 10.D-3
D_LITH              Thickness of lithosphere (m)    : 100.0D0
R_PLANET            Radius of planet (m)            : 80.0D0
GRAD_TYPE           Lithostatic gradient            : DEFAULT
LP_TOLER            Pressure tolerance              : 1.D-3
GRAV_V              Gravitational acceleration      : -5.D-5
------------------ Projectile ("Object") Parameters ----------------------
OBJNUM                number of objects             : 1
OBJRESH               CPPR horizontal               : 5
OBJRESV               CPPR vertical                 : 5
OBJVEL                object velocity               : -6.5D3
OBJMAT                object material               : impactr
OBJTYPE               object type                   : SPHEROID
------------------ Target Parameters -------------------------------------
LAYNUM                layers number                 : 1
LAYPOS                layer position                : 350
LAYMAT                layer material                : target_
LAYTPROF              thermal profile               : COND
EJECT_V               ejecta elevation              : 1.023
------------------ Time Parameters ---------------------------------------
DT                    initial time increment        : 2.0D-3
DTMAX                 maximum timestep              : 1.0D-1
TEND                  end time                      : 6.0D0
DTSAVE                save interval                 : 4.0D-2
------------------ Boundary Condition Parameters -------------------------
BND_L                 left                          : FREESLIP
BND_R                 right                         : FREESLIP
BND_B                 bottom                        : NOSLIP
BND_T                 top                           : OUTFLOW
------------------ Numerical Stability Parameters ------------------------
AVIS                  art. visc. linear             : 0.20D0
AVIS2                 art. visc. quad.              : 1.00D0
------------------ Tracer Particle Parameters ----------------------------
TR_QUAL               quality                       : 1
TR_SPCH               tracer spacing X              : 5.D0
TR_SPCV               tracer spacing Y              : 5.D0
TR_VAR                add. tracer fiels             : #TrP-TrT-TrA-TrV-Tr
------------------ (Material) Model parameters (global) ------------------
STRESS                Consider stress               : 1
PARTPRES              Pres. in part.                : 0
ADVECT                Advect by mass or volume      : 1
```

```
VEL_CUT                 Velocity cutoff                 : -4.D0
------------------ Data Saving Parameters ----------------------------
QUALITY                 Compression rate                : -50
VARLIST                 List of variables               : #Den-Tmp-Pre-Sie-Yl
--------------------------------------------------------------------
<<END
```

Model file 10% **1 kPa**

```
#ISINP
--------------------------------------------------------------------
--- this is the new input file used by iSALE versions of v7.0 and higher
------------------ General Model Info --------------------------------
VERSION                 __DO NOT MODIFY__               : 4.1
DIMENSION               dimension of input file         : 2
PATH                    Data file path                  : ./
MODEL                   Modelname                       : cg_dart04
TDUMP                   Dump save interval              : 1.0D-1
DUMP                    Restart with dump               : cg_dart03/00059.dum
REGRID                  Regridding                      : 0
------------------ Mesh Geometry Parameters --------------------------
GRIDH                   horizontal cells                : 0
: 300           : 40
GRIDV                   vertical cells                  : 40
: 600           : 0
GRIDSPC                 grid spacing                    : 1.023D-1
GRIDEXT                 ext. factor                     : 1.05d0
CYL                     Cylind. geometry                : 1.0D0
------------------ Global setup parameters ---------------------------
S_TYPE                  setup type                      : DEFAULT
T_SURF                  Surface temp                    : 288.0D0
DTDZSURF                Surface temp. gradient (K/m)    : 10.D-3
D_LITH                  Thickness of lithosphere (m)    : 100.0D0
R_PLANET                Radius of planet (m)            : 80.0D0
GRAD_TYPE               Lithostatic gradient            : DEFAULT
LP_TOLER                Pressure tolerance              : 1.D-3
GRAV_V                  Gravitational acceleration      : -5.D-5
------------------ Projectile ("Object") Parameters ------------------
OBJNUM                  number of objects               : 1
OBJRESH                 CPPR horizontal                 : 5
OBJRESV                 CPPR vertical                   : 5
OBJVEL                  object velocity                 : -6.5D3
OBJMAT                  object material                 : impactr
```

```
OBJTYPE              object type                    : SPHEROID
------------------ Target Parameters ------------------------------------
LAYNUM               layers number                  : 1
LAYPOS               layer position                 : 350
LAYMAT               layer material                 : target_
LAYTPROF             thermal profile                : COND
EJECT_V              ejecta elevation               : 1.023
------------------ Time Parameters --------------------------------------
DT                   initial time increment         : 2.0D-3
DTMAX                maximum timestep               : 1.0D-1
TEND                 end time                       : 7.5D0
DTSAVE               save interval                  : 4.0D-2
------------------ Boundary Condition Parameters ------------------------
BND_L                left                           : FREESLIP
BND_R                right                          : FREESLIP
BND_B                bottom                         : NOSLIP
BND_T                top                            : OUTFLOW
------------------ Numerical Stability Parameters -----------------------
AVIS                 art. visc. linear              : 0.20D0
AVIS2                art. visc. quad.               : 1.00D0
------------------ Tracer Particle Parameters ---------------------------
TR_QUAL              quality                        : 1
TR_SPCH              tracer spacing X               : 5.D0
TR_SPCV              tracer spacing Y               : 5.D0
TR_VAR               add. tracer fiels              : #TrP-TrT-TrA-TrV-Tr
------------------ (Material) Model parameters (global) -----------------
STRESS               Consider stress                : 1
PARTPRES             Pres. in part.                 : 0
ADVECT               Advect by mass or volume       : 1
VEL_CUT              Velocity cutoff                : -4.D0
------------------ Data Saving Parameters -------------------------------
QUALITY              Compression rate               : -50
VARLIST              List of variables              : #Den-Tmp-Pre-Sie-Yl
-------------------------------------------------------------------------
<<END
```

Material file 10% **100 kPa**

```
#ISMAT ! iSale material input file identification string for TEST1
-------------------------------------------------------------------
MATNAME     Material name                 : target_          : impactr
EOSNAME     EOS name                      : basalt_          : aluminu
EOSTYPE     EOS type                      : tillo            : tillo
```

STRMOD	Strength model	:	LUNDD	: JNCK
DILMOD	Dilatancy model	:	ALPHAPT	: NONE
DAMMOD	Damage model	:	IVANOV	: NONE
ACFL	Acoustic fluidisation	:	NONE	: NONE
PORMOD	Porosity model	:	WUNNEMA	: NONE
THSOFT	Thermal softening	:	OHNAKA	: JNCK
LDWEAK	Low density weakening	:	POLY	: NONE
----- Elastic strength parameters -----				
POIS	pois	:	2.5000D-01	: 3.3000D-01
----- Minimum Pr essure -----				
PMININ	minimum pressure	:	XXXXXXXXXX	: -2.440D+09
----- Thermal parameters -----				
TMELT0	tmelt0	:	1.9000D+03	: 9.3300D+02
TFRAC	tfrac	:	1.2000D+00	: 1.1590D+00
ASIMON	a_simon	:	6.0000D+09	: 6.0000D+09
CSIMON	c_simon	:	3.0000D+00	: 3.0000D+00
-------LUNDD parameters -----				
YDAM0	ydam0 (ycoh)	:	1.0000D+05	: XXXXXXXXXX
FRICDAM	fricdam	:	7.7000D-01	: XXXXXXXXXX
YLIMDAM	ylimdam	:	1.0000D+09	: XXXXXXXXXX
------IVANOV damage model parameters -----				
IVANOV_A	Damage parameter	:	1.0000D-04	: XXXXXXXXXX
IVANOV_B	Damage parameter	:	1.0000D-11	: XXXXXXXXXX
IVANOV_C	Damage parameter	:	3.0000D+08	: XXXXXXXXXX
----- Johnson-Cook strength parameters -----				
JC_A	strain coeff. a	:	XXXXXXXXXX	: 2.4400D+07
JC_B	strain coeff. b	:	XXXXXXXXXX	: 4.8800D+07
JC_N	strain exponent	:	XXXXXXXXXX	: 5.0000D-01
JC_C	str. rate coeff c	:	XXXXXXXXXX	: 2.0000D-02
JC_M	thermal soft.	:	XXXXXXXXXX	: 1.7000D+00
JC_TREF	ref. temperature	:	XXXXXXXXXX	: 2.9300D+02

ALPHACRIT	Critical distension	:	2.0D0	: XXXXXXXXXX
DILATCOEF	Max. dilatancy coef.	:	0.045D0	: XXXXXXXXXX
DILATPLIM	Zero dilat. coef. pressure	:	2.D8	: XXXXXXXXXX
DILATFRIC	Friction coef. at ALPHACRIT	:	0.4D0	: XXXXXXXXXX
---------porosity properties (Wuennemann) -----				
ALPHA0	Initial porosity	:	1.111D0	: XXXXXXXXXX
EPSE0	Elastic threshold	:	-2.0D-08	: XXXXXXXXXX
ALPHAX	Transition	:	1.05D+00	: XXXXXXXXXX
KAPPA	Exp Coefficient	:	7.6D-01	: XXXXXXXXXX
CHI	Sound speed ratio	:	0.8D-00	: XXXXXXXXXX

```
<<END ! used to identify the end of this file
```

Material file 10% **10 kPa**

```
#ISMAT ! iSale material input file identification string for TEST1
-------------------------------------------------------------
MATNAME     Material name                  : target_          : impactr
EOSNAME     EOS name                       : basalt_          : aluminu
EOSTYPE     EOS type                       : tillo            : tillo
STRMOD      Strength model                 : LUNDD            : VNMS
DAMMOD      Damage model                   : NONE             : NONE
ACFL        Acoustic fluidisation          : NONE             : NONE
PORMOD      Porosity model                 : WUNNEMA          : NONE
THSOFT      Thermal softening              : OHNAKA           : OHNAKA
LDWEAK      Low density weakening          : POLY             : NONE
----- Elastic strength parameters -------------------------------
POIS        pois                           : 2.5000D-01       : 3.3000D-01
----- Minimum Pr essure -----------------------------------------
PMININ      minimum pressure               : XXXXXXXXXX       : 1.3D+07
----- Thermal parameters ----------------------------------------
TMELT0      tmelt0                         : 1.9000D+03       : 9.3300D+02
TFRAC       tfrac                          : 1.2000D+00       : 1.1590D+00
ASIMON      a_simon                        : 6.0000D+09       : 6.0000D+09
CSIMON      c_simon                        : 3.0000D+00       : 3.0000D+00
-------LUNDD parameters-----------------------------------------
YDAM0       ydam0 (ycoh)                   : 1.0000D+04       : XXXXXXXXXX
FRICDAM     fricdam                        : 7.7000D-01       : XXXXXXXXXX
YLIMDAM     ylimdam                        : 1.0000D+09       : XXXXXXXXXX
----- VNMS strength parameters ----------------------------
YINT0       y0                             : XXXXXXXXXX       : 1.3000D+08
---------porosity properties (Wuennemann) ----------------------
ALPHA0        Initial porosity             : 1.1111D0         : XXXXXXXXXX
EPSE0         Elastic threshold            : -2.0D-08         : XXXXXXXXXX
ALPHAX        Transition                   : 1.05D+00         : XXXXXXXXXX
KAPPA         Exp Coefficient              : 7.6D-01          : XXXXXXXXXX
CHI           Sound speed ratio            : 0.8D-00          : XXXXXXXXXX
<<END ! used to identify the end of this file
```